Immunity-and-Matrix-Regulatory Cells Derived from Human Embryonic Stem Cells Safely and Effectively Treat Mouse Lung Injury and Fibrosis

Jun Wu[1,2,3,13], Dingyun Song[6,7,13], Zhongwen Li[1,2,3,13], Baojie Guo[1,2,3,4], Yani Xiao[11], Wenjing Liu[1,2,3], Lingmin Liang[1,2,3], Chunjing Feng[1], Tingting Gao[1,2,3], Zai Wang[8], Jianyan Wen[8,9], Shengnan Yang[6,10], Peipei Liu[6,7], Lei Wang[1,2,3], Yukai Wang[1,2,3], Liang Peng[8], Guihai Feng[1,2], Shiqiang Huang[1,2], Glyn Nigel Stacey[3,5], Wei Li[1,2], Yan Huo[11], Ronghua Jin[12], Qi Zhou[1,2,3,4], Liu Wang[1,2,3,*], Baoyang Hu[1,2,3,4*], Huaping Dai[6,7,*] and Jie Hao[1,2,3,*]

[1] State Key Laboratory of Stem Cell and Reproductive Biology, Institute of Zoology, Chinese Academy of Sciences, Beijing 100101, China

[2] Institute for Stem Cell and Regeneration, Chinese Academy of Sciences, Beijing 100101, China

[3] National Stem Cell Resource Center, Chinese Academy of Sciences, Beijing 100101, China

[4] University of Chinese Academy of Sciences, Beijing 100049, China

[5] International Stem Cell Banking Initiative, Hertfordshire, UK

[6] Department of Pulmonary and Critical Care Medicine, Center of Respiratory Medicine, China-Japan Friendship Hospital; National Clinical Research Center for Respiratory Diseases, Institute of Respiratory Medicine, Chinese Academy of Medical Sciences; Beijing 100029, China

[7] Graduate School of Peking Union Medical College, Chinese Academy of Medical Science and Peking Union Medical College, Beijing 100730, China

[8] Institute of Clinical Medical Sciences, Center of Respiratory Medicine, China-Japan Friendship Hospital, Beijing, China; Institute of Respiratory Medicine, Chinese Academy of Medical Sciences, Beijing, China

[9] Department of Cardiology, China-Japan Friendship Hospital; Beijing 100029, China

[10] Medical University of Ha Er Bin, Heilong Jiang Province, China

[11] National Center for Safety Evaluation of Drugs, National Institutes for Food and Drug Control, Beijing 100176, China

29 [12] Beijing Youan Hospital, Capital Medical University

30 [13] Co-first author

31 *Correspondence: haojie@ioz.ac.cn, byhu@ioz.ac.cn, daihuaping@ccmu.edu.cn,

32 wangliu@ioz.ac.cn

33

34 # Abstract

35 Lung injury and fibrosis represent the most significant outcomes of severe and acute lung disorders,
36 including COVID-19. However, there are still no effective drugs to treat lung injury and fibrosis. In this
37 study, we report the generation of clinical-grade human embryonic stem cells (hESCs)-derived
38 immunity- and matrix-regulatory cells (IMRCs) manufactured under good manufacturing practice (GMP)
39 requirements, that can treat lung injury and fibrosis in vivo. We generate IMRCs through sequentially
40 differentiating hESCs with xeno-free reagents. IMRCs possess a unique gene expression profile distinct
41 from umbilical cord mesenchymal stem cells (UCMSCs), such as higher levels of proliferative,
42 immunomodulatory and anti-fibrotic genes. Moreover, intravenous delivery of IMRCs inhibits both
43 pulmonary inflammation and fibrosis in mouse models of lung injury, and significantly improves the
44 survival rate of the recipient mice in a dose-dependent manner, likely through their paracrine functions.
45 IMRCs are superior to both primary UCMSCs and FDA-approved pirfenidone, with an excellent efficacy
46 and safety profile in mice, monkeys and two severely ill COVID-19 patients in our pilot study. In light
47 of recent public health crises involving pneumonia, acute lung injury (ALI) and acute respiratory distress
48 syndrome (ARDS), our findings indicate that IMRCs are ready for clinical trials on lung disorders.

49 **Introduction**

50 Lung injury is a serious threat to human health. It is caused by many chemical, physical and biological
51 factors, such as pneumonia, lung inflammation, and fibrosis. In a comprehensive analysis, the World
52 Health Organization ranks lung diseases as the second largest category, and predicts that by 2020, about
53 one fifth of human deaths will be attributed to lung diseases[1]. Acute lung injury (ALI) is the injury of

alveolar epithelial cells and capillary endothelial cells caused by various direct and indirect injury factors, resulting in diffuse pulmonary interstitial and alveolar edema, and acute hypoxic respiratory insufficiency. Pathophysiologically, its characteristics include decreased lung volume, decreased lung extensibility and imbalance of the ventilation / blood flow ratio. When ALI develops into the severe stage (oxygenation index < 200), it is called acute respiratory distress syndrome (ARDS). Globally, there are more than 3 million patients with ARDS annually, accounting for 10% of intensive care unit (ICU) admissions[2]. ALI / ARDS patients have an average mortality rate of 35-46%[3,4]. In late ARDS, pulmonary fibrosis (PF) develops due to persistent alveolar injury, repeated destruction, repair, reconstruction and over-deposition of extracellular matrix (ECM)[5], leading to progressive lung scars and common interstitial pneumonia. In general, idiopathic pulmonary fibrosis (IPF) patients show very poor prognosis, with a median survival time of 3-5 years after diagnosis[6]. It has also been reported that the degree of pulmonary fibrosis is closely related to the mortality of ARDS[7,8]. Importantly, there are still no effective FDA-approved drugs to treat ALI, ARDS or IPF hitherto, and most of the experimental drugs are still in Phase II or Phase III studies[2, 9,10].

Stem cell therapy is an emerging treatment modality being used to cure various inflammatory and/or degenerative diseases, including ALI and PF. In particular, mesenchymal stem cells (MSCs) have been tested as an intravenous infusion therapy for ALI and PF[11,12]. Preclinical and clinical studies of pulmonary fibrosis have shown that, after infusion, MSCs could migrate to the sites of lung injury, inhibit inflammation and improve recovery[13-15]. However, clinical studies with primary MSCs derived from the umbilical cord, bone marrow or adipose tissue have been hampered by the lack of available donors, limited cell numbers from each donor, donor and tissue heterogeneity, inconsistent cell quality and the lack of standardized cell preparations. Moreover, primary MSCs show limited self-renewal capacities and finite lifespans. MSC-like cells derived from human embryonic stem (hESCs)[16] could solve these problems[17-19], but the use of ill-defined and variable components of animal origin, such as fetal bovine serum (FBS) or OP9 feeder cells, may greatly compromise their consistency, safety and clinical applicability. Furthermore, these hESC-derived MSC-like cells have not been deeply characterized for their immunomodulatory functions in disease models.

In this study, we have used hESCs to derive immunity- and matrix-regulatory cells (IMRCs) that resemble MSCs in their capacity for self-renewal and tri-lineage differentiation. However, compared to primary umbilical cord mesenchymal stem cells (UCMSCs), IMRCs displayed a higher consistency in

quality, stronger immunomodulatory and anti-fibrotic functions, and a robust ability to treat lung injury and fibrosis in vivo.

Materials and methods

Generation of hESC-derived IMRCs

The hESC-derived IMRCs were generated by passaging cells that are migrating out from human embryoid bodies (hEBs), with xeno-free reagents. The clinical hESC line (Q-CTS-hESC-2) was prepared as described previously[20]. Clinical hESCs were maintained in commercially available Essential 8™ (E8) basal medium (Gibco, Carlsbad, MO, USA; A15169-01) with Essential 8™ Supplement (Gibco, A15171-01) on vitronectin-coated plates (1 μg/cm^2). To generate embryoid bodies (hEBs), hESCs were dissociated into small clumps by incubating at 37°C for 5 min with 1 mg/mL dispase (Gibco, 17105-04) and cultured to form hEBs for 5 days in KO-DMEM (Gibco, A12861-01) supplemented with 20% KOSR (Gibco, A3020902), 1× L-glutamine (Gibco, A12860-01), 1× NEAA (Gibco, 11140050) and 10 ng/mL bFGF (R&D systems, Minneapolis, MN, USA; 233-FB). Then, hEBs were transferred onto vitronectin-coated plates and cultured for 14 additional days. During this period, the outgrowth from the hEBs occurred. The outgrowth cells were dissociated by using Tryple (Gibco, A12859-01) and passaged at a low cell density of 1×10^4 cells per cm^2 in "IMRCs Medium" consisting of α-MEM (Gibco, 12561-049) supplemented with 5% KOSR, 1% Ultroser G (Pall corporation, New York, NY, USA; 15950-017), 1× L-glutamine, 1× NEAA, 10 ng/mL bFGF, 10 ng/mL TGF-β3 (R&D systems, 8420-B3) and 10 mg/L L-ascorbic acid (Sigma-Aldrich, St. Louis, MO, USA; A4403). Cells were passaged upon reaching approximately 80% confluence in IMRCs Medium. After 5 passages in culture, differentiated cultures were harvested for characterization. By this time, IMRCs displayed a fibroblastic morphology, expressed canonical "MSC-specific" surface markers including CD73, CD90, CD105 and CD29 and were negative for typical hematopoietic markers (CD45, CD34, HLA-DR)[21].

Isolation and culture of UCMSCs

Healthy full-term human placental samples were collected according to the policy of the Ethics Committee of the 306th Hospital of the Chinese People's Liberation Army, Beijing, China. Written informed consents were obtained from all donors before this study. All the samples were used in

accordance with standard experimental protocols approved by the Animal and Medical Ethical Committee of Institute of Zoology, Chinese Academy of Sciences, Beijing, China.

Briefly, the newborn umbilical cords of full-term pregnancies were obtained from the clinic and washed by PBS to remove all remnant blood. Then, the umbilical cords were cut to approximately 2 mm in size after removing the artery and vein. The pieces of umbilical cords were directly transferred into a 10 cm^2 culture flasks in α-MEM supplemented with 5% KOSR, 1% Ultroser G, 1× L-glutamine, 1× NEAA, 10 ng/mL bFGF and 10 mg/L L-ascorbic acid, and cultured in an atmosphere of 5% CO_2 at 37°C. UCMSCs were passaged upon reaching approximately 80% confluence. After 5 passages in culture, cells were harvested for characterization.

Cell culture

The clinical hESC line (Q-CTS-hESC-2) was prepared as described previously[20]. Clinical hESCs were maintained in the commercially available Essential 8™ (E8) basal medium on vitronectin-coated plates. Cells were passaged every 5 or 6 days using Versene (Gibco, A4239101). Clinical hESCs were tested weekly for mycoplasma contamination using a Myco-detection Kit (InvivoGen, San Diego, CA, USA; rep-pt1) and endotoxin contamination was tested using a ToxinSensor™ Chromogenic LAL Endotoxin Assay Kit (GenScript, Piscataway, NJ, USA; L00350). All cultures were maintained at 37°C, 5% CO_2 and atmospheric O_2 in a humidified incubator (Thermo Fisher Scientific, Waltham, MA, USA). A549 cells were purchased from Beina Biology (Shanghai, China). The cells were cultured in Ham's F-12K medium (Gibco, 21127022) with 10% fetal bovine serum (FBS; Gibco, 10091-148) at 37°C in 5% CO_2, and were treated with 10 ng/mL TGF-β1 (R&D systems, 240-B) or IMRCs conditioned medium where specified. To prepare the conditioned medium of IMRCs, IMRCs were cultured to 50% confluence in culture dishes, then, were changed to new medium. The conditioned medium was harvested after incubating IMRCs for 24 h.

Karyotyping

At passage 5, IMRCs were harvested. Karyotype analysis and G-binding were conducted at the Chinese Academy of Medical Science & Peking Union Medical College (Beijing, China).

137 **RNA-seq library preparation and data analysis**

138 Total RNA was isolated from hESCs, IMRCs and UCMSCs by Trizol (Invitrogen, Waltham, MA, USA;
139 15596018). RNA-seq libraries were prepared with the NEBNext®Ultra™ RNA Library Prep Kit for
140 Illumina®. Sequencing was performed on an Illumina HiSeq X-Ten sequencer with 150 bp paired-end
141 sequencing reaction. The bulk RNA-Seq data for hESCs were downloaded from GEO database[22]. All
142 RNA-sequencing data analysis was performed with Hisat2 (version 2.1.0)[23] and Cufflinks (version
143 2.2.1)[24] using the UCSC hg19 annotation with default settings. Reads with unique genome locations and
144 genes with no less than 1 FPKM in at least one sample were used for the next step of analysis. Two-fold
145 change was used as the threshold to filter for differentially expressed genes (DEGs) i.e. increased or
146 decreased expression of less than 2-fold was not considered significant. Clustering, heatmap, Venn
147 diagram and scatterplots analysis were performed with hierarchical cluster and heatmap.2 functions in
148 R. Pearson correlation coefficient was calculated by cor.test in R. Gene set enrichment analysis were
149 performed by GSEA[25].

150 **Flow cytometry**

151 Cells were harvested and blocked with 2% bovine serum albumin (BSA; Sigma-Aldrich, B2064) for 20
152 min at room temperature. Then, the cells were stained with fluorescein-conjugated antibodies for 40 min
153 at room temperature in 1% BSA. After incubation, cells were washed 3 times and analyzed with MoFlo
154 (Beckman, Brea, CA, USA) and associated software. The antibodies used for flow cytometry were as
155 follows: PE-conjugated mouse anti-human CD29 (Biolegend, San Diego, CA, USA; 303004), PE-
156 conjugated mouse anti-human CD73 (BD Biosciences, San Jose, CA, USA; 550257), PE-conjugated
157 mouse anti-human CD90 (eBioscience, San Diego, CA, USA; 12-0909-42), PE-conjugated mouse anti-
158 human CD105 (Biolegend, 323206), PE-conjugated mouse anti-human CD34 (BD Biosciences, 555822),
159 PE-conjugated mouse anti-human CD45 (BD Biosciences, 560957), PE-conjugated mouse anti-human
160 HLA-DR (BD Biosciences, 555561), and the PE-conjugated mouse IgG1 (BD Biosciences, 551436) as
161 an isotype control.

162 **Trilineage differentiation**

Osteogenic, adipogenic, and chondrogenic differentiation experiments were performed following the instructions of the human mesenchymal stem cell functional identification kit (R&D systems, SC006). For osteogenic differentiation, 4.2×10^3 cells were seeded per well in 96-well plates. When cells reached 50–70% confluency, the medium was replaced with osteogenic differentiation medium and kept for 3 weeks. To assess osteogenic differentiation, immunofluorescence (Osteocalcin) and Alizarin Red S (Sigma-Aldrich, A5533) staining was performed for the calcium-rich extracellular matrix. For adipogenic differentiation, cells were seeded into a 24-well plate at the density of 3.7×10^4 cells/well, and maintained in culture medium until 100% confluency. Then, cells were cultured in adipogenic differentiation medium for 3 weeks. Lipid droplets of the resultant differentiated cells were detected using immunofluorescence (AFBP-4) and Oil red O (Sigma-Aldrich, O0625) staining. For chondrogenic differentiation, 2.5×10^5 cells resuspended in chondrogenic differentiation medium were centrifuged for 5 min at 200×g in a 15-mL conical tube (Corning, NY, USA). Then, cells were cultured for 3 weeks. After 3 weeks, chondrogenic pellet was harvest and fixed in 4% paraformaldehyde (Aladdin Chemical Co., Ltd., Shanghai, China; C104190). Cryosectioning was performed by OTF Cryostat (Leica, Germany) and 10 μm sections were stained with immunofluorescence (Aggrecan) and Alcian Blue (Sigma-Aldrich, A5268) staining.

Growth curve

IMRCs and UCMSCs were seeded onto 96-well plates at a density of 8×10^3 cells per well. Cell Counting Kit-8 (CCK8; Thermo Fisher Scientific, CK04) was used to measure the cells' growth. CCK8 solution was added at day 1, day 3, day 5 and day 7 by following the CCK8 kit manufacturer's protocol. After 2 h of incubation, absorbance was measured at 450 nm.

Cell diameter analysis

The IMRCs and UCMSCs were harvested at passage 5 and the cell diameters were measured with Image J software (NIH) software analysis. Normal Distribution curves were fitted to the cell diameter data to analyze the cell size distribution characteristics.

Cell viability test

189 The IMRCs and UCMSCs were cryopreserved in a published clinical injection[26] for 15 days in liquid
190 nitrogen. After complete recovery of the cells, cells were suspended in clinical injection and remained
191 under 4°C. Then, cell viability was determined using 0.4% (w/v) Trypan Blue (Gbico, 15250061) at
192 different time points by a Cell Counter (Invitrogen, Countess II) using the average of 3 replicates.

193 **Single-cell RNA-seq library preparation & sequencing**

194 IMRCs and UCMSCs were harvested and suspended in PBS. Then, cell suspensions were loaded onto
195 the Chromium Single Cell Controller (10× Genomics) to generate single Gel Beads-in-Emulsion (GEMs)
196 by using Single Cell 30 Library and Gel Bead Kit V2 (10× Genomics, 120237). Cells were lysed and the
197 released RNA was barcoded through reverse transcription in individual GEMs. Following reverse
198 transcription, cDNAs with both barcodes were amplified, and a library was constructed using the Single
199 Cell 30 Reagent Kit (v2 chemistry) for each sample following the manufacture's introduction.
200 Sequencing was performed on an Illumina NovaSeq 6000 System in the 2 × 150 bp paired-end mode.
201 Raw files were processed with Cell Ranger using default mapping arguments. Gene expression analysis
202 and cell type identification were performed by Seurat V3.1. Briefly, after normalizing and quality control,
203 the tSNE was used for non-linear dimensional reduction. The figures were produced by DimPlot and
204 VlnPlot functions in Seurat.

205 **Cell culture with IFN-γ treatment**

206 Cells at passage 4 were digested and seeded into 6-well plates. IMRCs were seeded at a density of 3 ×
207 10^5 cells / well, and UCMSCs were seeded at a density of 2 × 10^5 cells / well. After adherence for 24h,
208 IFN-γ (0, 25, 50, 100 ng/mL) (R&D systems, 285-IF) was added into the culture medium to culture for
209 24h. Cells and conditioned medium were harvested after IFN-γ stimulation for qPCR and cytokine
210 analysis.

211 **Cytokine analysis**

212 Conditioned medium of UCMSCs and IMRCs were collected after IFN-γ (100 ng/mL) stimulation for
213 24h. Forty-eight cytokines including FGF basic, Eotaxin (also known as CCL11), G-CSF (CSF3),
214 GMCSF (CSF2), IFN-γ, IL-1β, IL-1ra, IL2, IL4, IL5, IL6, IL7, IL8 (also known as CXCL8), IL9, IL10,

215 IL12 (p70), IL13, IL15, IL17A, IP10 (CXCL10), MCP1 (CCL2), MIP-1α (CCL3), MIP-1β (CCL4),
216 PDGFB, RANTES (CCL5), TNF-α, VEGF, IL-1α, IL-2Rα, IL-3, IL-12 (p40), IL-16, GRO-α, HGF, IFN-
217 α2, LIF, MCP-3, MIG, β-NGF, SCF, SCGF-β, SDF-1α, CTACK, MIF, TRAIL, IL-18, M-CSF, TNF-β
218 were detected by using the premixed 48-plex Bio-Plex Pro Human Cytokine Assay (Bio-Rad, Hercules,
219 CA, USA; 12007283) according to the manufacturer's instructions.

220 **Real-time quantitative PCR**

221 For reverse transcription (RT), RNA was extracted using an RNAprep Pure Cell/Bacteria Kit (TIANGEN,
222 Beijing, China; DP430). Two micrograms of RNA were reverse transcribed into cDNA using a
223 PrimeScript™ First-Strand cDNA Synthesis Kit (TaKaRa, Shiga, Japan; 6110B). Real-time quantitative
224 PCR (qPCR) was performed and analyzed using a Stratagene Mx3005P system (Agilent Technologies,
225 Santa Clara, CA, USA) with SYBR Green Real-Time PCR Master Mix Plus (Toyobo, Osaka, Japan;
226 QPS-201). *GAPDH* was used for internal normalization.

227 **Enzyme-linked immunosorbent assay (ELISA)**

228 To determine the secretion of human MMP1, cell culture supernatants were collected after 48 hours of
229 culture. The levels of human MMP1 protein were measured by a Human MMP1 ELISA Kit (Cusabio,
230 Wuhan, China; CSB-E04672h) according to the manufacturer's instructions. Concentrations of TNF-α
231 (Expandbio, Beijing, China; Exp210030) and TGF-β1 (Expandbio, Exp210089) in the mouse lung
232 homogenates were measured using ELISA kits according to the manufacturer's instructions.

233 **Human MMP1 activity**

234 To determine the activity of human MMP1, cell culture supernatants were collected after 48 hours of
235 culture. The activity of human MMP1 were measured by a SensoLyte ® Plus 520 MMP-1 Assay Kit
236 (AnaSpec, San Jose, CA, USA; AS-72012) according to the manufacturer's instructions. A specific anti-
237 MMP-1 monoclonal antibody was used in combination with an MMP1 fluorogenic substrate, 5-
238 FAM/QXL®520 FRET peptide. The fluorescence signal is monitored at Ex/Em = 490 nm/520 nm upon
239 MMP-1-induced cleavage of the FRET substrate.

240 **Immunofluorescence staining**

241 Cells were fixed with 4% paraformaldehyde for 15 min, permeabilized with 0.5% Triton X-100 for 15
242 min and blocked with 2% BSA for 60 min at room temperature. Then, the cells were stained with 1:200
243 mouse monoclonal IgG E-cadherin (Abcam, San Francisco, CA, USA; ab1416), 1:200 rabbit monoclonal
244 IgG Collagen I (Cell Signaling Technology, Danvers, MA, USA; 84336), 1:200 rabbit anti-FABP-4
245 (Thermo Fisher Scientific, PA5-30591), 1:200 rabbit anti-Osteocalcin (Thermo Fisher Scientific, PA5-
246 11849), 1:200 mouse anti Aggrecan (Thermo Fisher Scientific, MA3-16888) overnight at 4°C in 2%
247 BSA in PBS. The cells were washed three times with PBS and then incubated with 1:200 Alexa Fluor
248 488 donkey anti-mouse IgG (H+L) (Jackson ImmunoResearch, West Grove, PA, USA; 715-545-151),
249 1:200 Fluorescein (Cy3) donkey anti-rabbit IgG (H+L) (Jackson ImmunoResearch, 711-165-152), 1:200
250 Fluorescein (Cy3) donkey anti-mouse IgG (H+L) (Jackson ImmunoResearch, 715-165-151) or
251 Fluorescein (Cy2) donkey anti-rabbit IgG (H+L) (Jackson ImmunoResearch, 711-545-152) secondary
252 antibodies in 2% BSA for 60 min at room temperature in the dark. The washing step was repeated before
253 staining the nuclei with Hoechst 33342 (Invitrogen, H3570).

254 **Western blot**

255 Cells were harvested in RIPA Lysis Buffer (strong) (CWbio, Taizhou, China; CW2333S) containing
256 protease inhibitors (Roche, 4693124001). A total of 40 μg proteins were separated by 4-20% gradient
257 SDS-PAGE gels (GenScript, M42015C) and transferred to PVDF membranes (Millipore, Billerica, MA,
258 USA; IPVH00010). The membranes were blocked at room temperature with 1% BSA for 1 h and
259 incubated overnight at 4°C with primary antibodies: rabbit Collagen I antibody (Cell Signaling
260 Technology, 84336), mouse E-cadherin antibody (Abcam, ab1416) and mouse β-actin antibody (Sigma-
261 Aldrich, A1978). Then, the membranes were washed with TBST for 3 times and incubated for 1 h with
262 a secondary antibody: anti-mouse IgG antibody (HRD) (Sigma-Aldrich, A9044) and anti-rabbit IgG
263 antibody (HRD) (Sigma-Aldrich, A0545) at room temperature. Images were obtained using the
264 ChemiDoc XRS+ imaging system (Bio-Rad) and quantified using the Quantity One software.

265 **Soft agar colony formation assay**

266 Soft agarose gels were prepared according to previously published protocols[27]. Cells were harvested and
267 diluted to a cell concentration of 2.5×10^4/mL, before mixing with the agarose mixture in 6-well culture

268 plates. The plates were incubated in a 37°C incubator for 21 days.

269 **Animals**

270 Adult female and male cynomolgus monkeys (3–5 years old) were housed in single quarters with a 12/12-
271 hr light/dark cycle. Animals were provided with monkey chow and enrichment food twice a day and
272 water *ad libitum*. The monkey experiments were performed at the National Center for Safety Evaluation
273 of Drugs, National Institutes of Food and Drug Control (Beijing, China). The Institutional Animal Care
274 and Use Committee of the National Center for Safety Evaluation of Drugs approved all monkey studies
275 (NO. IACUC- 2018- k001).
276 Specific pathogen-free (SPF) 11- to 13-week-old C57BL/6 male mice were purchased from the Animal
277 Center of Peking University (Beijing, China). All experimental and control mice were weight-matched,
278 and their weights ranged from 25 to 30 g. All mice were housed in the animal care facility of the Institute
279 of Medical Science, China-Japan Friendship Hospital. Mice were maintained under SPF conditions at
280 room temperature (between 20–24°C), with humidity between 35–55%, in a 12/12 h light/dark cycle,
281 with food and water *ad libitum* and monitored with respect to their general state, fur condition, activity,
282 and weight according to institutional guidelines. The mice were sacrificed at each observational time
283 point by using intraperitoneal pentobarbital overdose. The Animal Studies Committee of the China-Japan
284 Friendship Hospital (Beijing, China) approved all mice studies (NO.190108).

285 **Acute toxicity and long-term toxicity test**

286 Acute toxicity test: Low dose (2.6×10^6), middle dose (2.6×10^7) and high dose (1×10^8) IMRCs were
287 infused into cynomolgus monkeys (3-5 years old) by single intravenous infusion. After 6 months, their
288 body weight, ophthalmology status, hematology, blood chemistry and urine chemistry were measured.
289 Long-term toxicity test: High dose (1×10^7) and low dose (2.6×10^6) IMRCs, or saline, were injected into
290 cynomolgus monkeys (3-5 years old) by intravenous infusion once a week for 22 times, after which their
291 body weight, body temperature, food intake and organ weights were measured.

292 **Copy number variation calling**

293 30X whole-genome sequencing data was produced by HiSeq X-Ten (Annoroad Gene Technology Co.,

294 Ltd) and used to analyze single nucleotide mutation changes between IMRCs and hESCs. As previously
295 described[28], the whole-genome sequencing data was mapped to the hg19 reference genome by BWA
296 (version 0.7.15) using the 'mem' mode with default parameters. The genome coverage were calculated
297 by bedtools[29]. The normalized coverage depth for each bin was calculated by dividing the raw coverage
298 depth by the average sequencing depth. Duplicate reads were removed and the uniquely mapped reads
299 were retained for the copy-number variation (CNV) analysis, in which chromosomal sequences were
300 placed into bins of 500 kb in length. The repeat regions annotated for hg19 genome by RepeatMasker
301 (http://www. repeatmasker.org) were removed from the genomic sequence before calculating the
302 coverage. The CNV scatterplot was drawn using ggplot2.

303 **Histological staining and immunostaining staining analysis**

304 Mouse lung histology was performed as follows. Briefly, the lung was dehydrated, paraffin-embedded
305 and cut into 4 μm sections. Lung sections were stained with H&E and Masson's trichrome stain for
306 assessment of pathological changes. Immunohistochemical staining was performed using antibodies
307 against α-SMA (Servicebio, Wuhan, China; GB13044), Fibronectin (Servicebio, GB13091), Collagen I
308 (Servicebio, GB13091) and GFP (Servicebio, GB13227). Immunofluorescence staining was performed
309 using antibodies against GFP (Servicebio, GB13227), CD31 (Servicebio, GB11063-3) and SPC
310 (Millipore, AB3786).

311 **Labeling IMRCs with DiR dye**

312 IMRCs were labeled with a lipophilic, near-infrared fluorescent dye 1,1-dioctadecyl- 3,3,3,3-tetramethyl
313 indotricarbocyanine iodide (DiR; YEASEN, Shanghai, China; 40757ES25). IMRCs were suspended at
314 a concentration of 1×10^6 cells / mL and incubated with DiR buffer for 20 min at 37°C according to the
315 manufacturer's protocol. After incubation, cells were centrifuged at 1000-1500 rpm for 5 min. After
316 washing twice with PBS and resuspension, the IMRCs were preheated at 37°C before infusion. Both
317 DiR-labeled and unlabeled cells (5×10^6 in 200 μL saline) were injected via the tail vein.

318 **In vivo imaging of IMRCs' biodistribution**

319 Mice were lightly anesthetized and were monitored using the in vivo imaging systems at 0 day, 1 day, 3

320 days, 5 days, 7 days, 9 days, 15 days, 21 days, 27 days, 32 days, 37 days and 46 days after tail intravenous
321 injection of DiR-labeled IMRCs (5×10^6 cells in 200 μL saline). Serial fluorescence images were also
322 obtained in major organs ex vivo. In order to reduce autofluorescence, the ideal filter conditions for DiR
323 imaging were an excitation/emission spectrum in the near infrared range (750/780 nm)[30,31].

324 **Lung function**

325 The flexiVentFX experimental platform was set up according to the manufacturer's instructions. On the
326 twenty-first day, after 3% pentobarbital sodium (40 mg/kg) intraperitoneal injection of anesthesia, mice
327 were fixed supine within five to eight minutes, and endotracheal intubation was inserted in the middle of
328 a tracheotomy. After computer processing, indicators of lung function required were obtained, including
329 the inspiratory capacity (IC), respiratory resistance (Rrs), static compliance (Crs), elastic resistance (Ers),
330 Newtonian resistance, tissue damping (G), tissue elasticity (H) and forced vital capacity (FVC)[32].

331 **Lung coefficient**

332 The lung tissue was completely removed, weighed by electronic balance, and the lung coefficient was
333 calculated according to the formula: wet lung weight (g) / total body weight (kg).

334 **Cell therapy in BLM mouse model of pulmonary fibrosis**

335 The BLM mouse model was generated by intratracheal injection of 1.5 $mg.kg^{-1}$ bleomycin sulphate
336 (BLM; Bioway, China; DP721) in normal saline under light anaesthesia. The IMRCs were delivered
337 intravenously at 0 day or 1 day or 7 days or 14 days after injury. Mice were euthanized with 50 mg/mL
338 sodium pentobarbital (0.6 mg/10 g weight) according to published guidelines[33]. Animals were killed 21
339 days after BLM injury. After perfusion with normal saline, the left lungs were used for morphometric
340 analysis while the right lungs were removed and used for other analyses.

341 **Micro-CT**

342 Mouse CT scans were performed according to the manufacturer's instructions.

343 **Compassionate use study of two severely ill COVID-19 patients**

344 We conducted a pilot study using GMP-grade IMRCs, under an expanded access program for
345 compassionate use in COVID-19 patients. The pilot study was approved by the Ethics Committee of the
346 Beijing Youan Hospital, Capital Medical University (LL-2020-010-K, Youan EC [2020]005). After two
347 severely ill COVID-19 patients, who tested positive for SARS-CoV-2 by qRT-PCR and were diagnosed
348 with ALI (aged 44–46 yrs; 1 male and 1 female), gave their consent and met the eligibility criteria, their
349 serum samples were collected and processed in accordance with the ethical legislation and the guidelines
350 of the Ethics Committee of the Beijing Youan Hospital, Capital Medical University.

351 **Statistics**

352 All data are expressed as mean ± SEM. Survival curves were derived by the Kaplan-Meier method and
353 compared via generalised Wilcoxon test. Statistical analysis was performed using GraphPad Prism 5.0
354 statistical software (San Diego, CA, USA). The statistical significance of multiple groups was compared
355 to each other using Tukey's multiple comparison test ANOVA. A p value of <0.05 was considered
356 statistically significant.
357

358 **Results**

359 **Generation of hESC-derived IMRCs**

360 In this study, hESC-derived IMRCs were generated by passaging cells that are migrating from human
361 embryoid bodies (hEBs), using xeno-free reagents (Fig. 1A and 1B). The clinical hESC line (Q-CTS-
362 hESC-2) was prepared as described previously[20]. Clinical hESCs were maintained in Essential 8™ basal
363 medium (E8) on vitronectin-coated plates, before dissociation into small clumps to form hEBs for 5 days.
364 Then, hEBs were transferred onto vitronectin-coated plates and cultured for 14 additional days. The hEBs
365 outgrowth cells were dissociated and passaged continuously in IMRCs Medium. After 5 passages,
366 IMRCs were harvested for characterization. IMRCs possessed fibroblast-like morphology (Fig. 1B) and
367 maintained diploid karyotypes at passage 5 (Fig. 1C). Moreover, copy-number variation analysis by
368 whole genome sequencing data also indicated no chromosome aneuploidies, large deletions nor
369 duplication fragments were detected (Fig. 1D). Next, we analyzed the expression profile of MSC-specific
370 genes (Fig. 1E). IMRCs showed a pattern that greatly differed from hESCs, and closely resembled

371 primary umbilical cord-derived MSCs (UCMSCs). All pluripotency genes (*POU5F1*, *SOX2, NANOG,*
372 *ZFP42, SALL4*), mesendoderm genes (*MIXL1*), and ectoderm genes (*GAD1, GFAP*) were extinguished
373 in both IMRCs and UCMSCs (Fig. 1E). IMRCs expressed MSC-specific genes, including *PDGFRA* and
374 *SPARC,* and the MSC-specific surface markers *NT5E* (CD73), *ENG* (CD90), *THY1* (CD105) and *ITGB1*
375 (CD29). Flow cytometry analysis further confirmed this surface marker profile (Fig. 1F, Fig.S1A, B). By
376 contrast, IMRCs were negative for the hematopoietic surface markers *PTPRC* (CD45) and CD34. IMRCs
377 displayed the ability to undergo tri-lineage differentiation into mesenchymal tissues, such as adipose,
378 cartilage and bone cells (Fig. 1G, Fig.S1C). The proliferation rate of IMRCs was higher than that of
379 UCMSCs at passage 15, suggesting that IMRCs have a stronger capacity for long-term self-renewal (Fig.
380 1H). Interestingly, IMRCs were generally smaller than UCMSCs (Fig. 1I), suggesting that IMRCs can
381 pass through smaller blood vessels and capillaries more easily, and are thus may be less likely to cause
382 pulmonary embolism. To evaluate the clinical potential of the IMRCs, we measured the viability of
383 IMRCs suspended in a published clinical injection buffer at 4°C. We found that the viability of IMRCs
384 remained higher (93%) than UCMSCs (73%) after 48h (Fig. 1J).

385 **IMRCs possess unique gene expression characteristics**

386 To clarify the degree of similarity between hESCs, IMRCs and primary UCMSCs at the whole
387 transcriptome level, we performed genome-wide profiling of IMRCs and UCMSCs and compared their
388 gene expression with hESCs[22]. Whole-transcriptome analysis confirmed that IMRCs clustered together
389 with UCMSCs in an unsupervised hierarchical clustering (Fig. 2A). Accordingly, MSC-specific genes
390 such as *NT5E, ENG, PDGFRA, SPARC* and *ITGB1* were upregulated whereas pluripotency genes such
391 as *POU5F1, SOX2, SALL4* and *ZFP42* were extinguished in IMRCs, relative to hESCs, and the overall
392 correlation with hESCs was weak (R^2=0.66, Fig. 2B). Next, we analyzed for the expression of genes
393 specific to IMRCs, compared to UCMSCs (Fig. 2C). While the overall correlation with UCMSCs was
394 stronger (R^2=0.87), we also found that many genes were differentially expressed in IMRCs compared to
395 UCMSCs. The upregulated genes promote immunomodulation (*LIF*), tissue repair (*VEGFA, GREM1*),
396 cell division (*CDC20*) and anti-fibrosis (*MMP1*). By contrast, the downregulated genes predominantly
397 promote inflammation (*IL-1B, CXCL8, CCL2* and *CXCL1;* Fig. 2C). Gene set enrichment analysis
398 (GSEA) of the differentially expressed genes confirmed that IMRCs manifest reduced inflammation and

399 stronger proliferative capacity as their top gene signatures, compared to primary UCMSCs (Fig. 2D-E,
400 Fig. S2).
401 To elucidate the heterogeneity of gene expression amongst IMRCs, single cell RNA sequencing
402 (scRNAseq) was performed for both IMRCs and primary UCMSCs. Our scRNAseq data also showed
403 that IMRCs were relatively homogenous in expression for the MSC-specific markers *PDGFRA, SPARC,*
404 *NT5E, ITGB1* and *ENG.* IMRCs were also relatively homogenous in their suppression of pluripotency
405 and non-mesenchymal markers, relative to hESCs and UCMSCs, suggesting they are likely to be similar
406 in biological activity to primary MSCs after transplantation (Fig. 2F). These results provided insight into
407 the clinical applicability of IMRCs, especially with regards to their complete loss of pluripotency and
408 their gain in hyper-immunomodulatory potential.

409 **IMRCs treated with IFN-γ show hyper-immunomodulatory potency**

410 To test the immunomodulatory capacity of IMRCs, we exposed them to the pro-inflammatory cytokine
411 IFN-γ. We found that after stimulation with IFN-γ, both primary UCMSCs and IMRCs displayed similar
412 characteristic morphological changes (Fig. 3A). IFN-γ stimulation also potently upregulated *IDO1*
413 expression in both primary UCMSCs and IMRCs, but much more significantly so in IMRCs (Fig. 3B).
414 This is important because *IDO1* (indoleamine 2, 3-dioxygenase 1) has been shown to mediate
415 immunosuppression in T cell-inflamed microenvironments through its catabolism of tryptophan and thus
416 suppression of the tryptophan–kynurenine–aryl hydrocarbon receptor (Trp–Kyn–AhR) pathway in T
417 cells. To further characterize IMRCs at a molecular level, we conducted genome-wide RNA profiling to
418 compare IMRCs with UCMSCs, after IFN-γ stimulation (Fig. 3C). Hierarchical clustering revealed that
419 IMRCs clustered separately from UCMSCs, although they appeared more similar after IFN-γ stimulation
420 (Fig. 3D). To analyse IMRCs after IFN-γ stimulation in greater detail, we separated their differentially
421 expressed genes into different categories and tested their overlap using Venn diagram analysis (Fig. 3E).
422 We found that some pro-inflammatory genes showed lower expression while some pro-regenerative
423 genes showed higher expression levels in IMRCs, compared to primary UCMSCs (Fig. 3F).
424 To confirm these findings, we performed a focused ELISA analysis of 48 biologically relevant
425 chemokines and cytokines in the secretomes of both stimulated IMRCs and UCMSCs. We found that at
426 least nine pro-inflammatory cytokines were lower in IMRCs than UCMSCs, including interleukin-6 (IL-

427 6), IL-1b, tumor necrosis factor alpha (TNF-α), GRO-α, IFN-α2, IL-1α, IL-3, and IL-8 (Fig. 3G and
428 Fig. S3). Furthermore, while the anti-inflammatory IL-4 was lower, the immunomodulatory cytokines
429 IL-1RA, LIF, and RANTES were higher in IMRCs than UCMSCs (Fig. 3H). Amongst the pro-
430 regenerative cytokines, we found that GM-CSF was similar while VEGFA, MIG and SDF-1a were higher
431 in IMRCs than UCMSCs (Fig. 3I). These results indicate that IMRCs manifest much stronger
432 immunomodulatory and pro-regenerative functions than UCMSCs.

433 **IMRCs suppress the pro-fibrotic effects of TGF-β1**

434 Our scRNAseq results also indicated that more than 99% of IMRCs expressed *MMP1* compared with
435 primary UCMSCs (<1%) (Fig. 4A). Similarly, gene expression analysis by RT-qPCR showed that IMRCs
436 express much higher levels of *MMP1* than hESCs, UCMSCs or human foreskin fibroblasts (HFF; Fig.
437 4B). MMP1 could be detected as a highly secreted protein in the conditioned media of IMRCs by ELISA
438 (Fig. 4C). In addition, the secreted MMP1 was an enzymatically active and correctly processed isoform
439 (Fig. 4D, E). To investigate the role of the IMRCs on fibrosis, the human epithelial cell line A549 was
440 used to establish an in vitro fibrosis model. The morphology of A549 cells became myofibroblast-like
441 after 48h treatment with 10 ng/mL TGF-β1 (Fig. 4F). Consistent with the morphological changes, the
442 expression of myofibroblast markers such as *ACTA2*, *Collagen I*, *Collagen II*, *Fibronectin* and *TGFB1*
443 increased, while the expression of the epithelial identity marker *CDH1* was extinguished, suggesting that
444 the A549 cells had undergone TGF-β1-induced myofibroblast transdifferentiation (Fig. 4G).
445 Immunofluorescence and western blot analyses confirmed that TGF-β1 induced the upregulation of
446 collagen I and the downregulation of E-cadherin (Fig. 4H, I). These results indicated that the A549
447 alveolar epithelial cells could simulate lung fibrosis in vitro. Thereafter, A549 cells were cultured with
448 or without the conditioned media of IMRCs, along with TGF-β1 treatment. Our results showed that the
449 IMRCs conditioned media significantly ameliorated the induction of *Collagen I* expression (Fig. 4J).
450 Immunofluorescence and western blot analyses further confirmed that IMRCs conditioned media could
451 extinguish Collagen I protein expression during the A549-to-myofibroblast transdifferentiation (Fig. 4K,
452 L, M). These results suggested that IMRCs might be able to inhibit lung fibrosis.

453 **Safety evaluation of IMRC transfusion into mice and monkeys**

454 Tumorigenicity has long been an obstacle to the clinical application of cells derived from hESCs, due to
455 the contamination of residual hESCs that could form teratomas. Our single cell RNA sequencing showed
456 that no residual OCT4/SOX2/NANOG/TERT/DPPA5^{+} hESCs remained amongst the IMRCs, and that
457 all pluripotency gene expression had been extinguished (Fig. 5A). To ensure their short-term and long-
458 term safety, a series of biosafety-related experiments were performed according to the "Guidelines for
459 Human Somatic Cell Therapies and Quality Control of Cell-based Products" of China Food and Drug
460 Administration (CFDA) (http://samr.cfda.gov.cn/WS01/CL0237/15709.html), whereupon the IMRCs
461 were verified as suitable for use in human therapy (Supplementary Table S1). These biosafety-related
462 experiments included testing for bacteria, fungi, mycoplasma, virus (by in vivo and in vitro methods),
463 pluripotent cell residuals, tumorigenicity and biopreparation safety (endotoxin and bovine serum albumin
464 residuals). According to these tests, the safety of the IMRCs has been verified as required by the National
465 Institutes for Food and Drug Control (NIFDC) in China.
466 To track the biodistribution and long-term engraftment of IMRCs in vivo, whole-animal imaging of mice
467 was performed at designated time points (day 0, 1, 3, 5, 7, 9, 15, 21, 27, 32, 37 and 46) after injection
468 with DiR-labeled IMRCs. Our data showed that DiR fluorescence intensity declined by half on the 5th
469 day, and dropped steadily over at least 15 days, disappearing around day 46 (Fig. 5B, C and Fig. S4C).
470 No DiR fluorescence signals were observed in the control mouse. These results indicate that IMRCs
471 never show long-term engraftment in vivo. However, IMRCs were predominantly distributed to the lung,
472 with small amounts in the liver and spleen (Fig. S4B). To assess the recruitment of IMRCs to the lung,
473 GFP-labeled IMRCs were used to track the distribution of IMRCs. A number of GFP-labeled IMRCs
474 were observed in the interstitial spaces in the lung, but not in the lung capillaries (Fig. 5D).
475 Immunofluorescence analysis of the expression of the alveolar type II epithelial cell marker SPC and the
476 endothelial cell marker CD31 showed that neither marker was co-expressed with GFP-labeled IMRCs in
477 the lungs of mice by day 21 (Fig. 5D). These data suggested that IMRCs are unlikely to engraft nor
478 transdifferentiate into endothelial or epithelial cells, after homing to the interstitium of lung tissues in
479 vivo.
480 To give some indication of the tumorigenic potential of IMRCs in vitro, a soft agar assay was performed
481 (Fig. 5E). As a positive control, the PANC-1 pancreas tumor cell line showed a colony formation rate of
482 about 30%. A small number of clones were also formed in hESCs, and the colony formation rate was
483 about 0.5%. However, no colonies were formed by IMRCs. These results indicated that IMRCs had no

484 tumorigenic potential as determined by this assay. Somatic mutation analysis by whole genome
485 sequencing also showed zero mutations in all coding and noncoding exon regions of the IMRCs genome
486 (Fig. 5F). Tumor formation assays also confirmed that IMRCs could not form any tumors in
487 immunodeficient mice after injection in vivo (Supplementary Table S1).
488 We also transfused different doses of IMRCs into cynomolgus monkeys (*Macaca fascicularis*), to
489 evaluate the short- and long-term toxicity of IMRCs in primates. After 6 months, acute toxicity data
490 showed that all blood biochemistry and urinalysis markers remained in the normal range (Fig. 5G, H),
491 indicating normal liver, kidney, heart, muscular, pancreatic and overall metabolic functions. Moreover,
492 no abnormalities were observed in the long-term toxicity tests either (Fig. S5B, n=18). These results
493 indicated that IMRCs have a robust safety profile in in vitro and in vivo animal models and could
494 potentially provide therapeutic treatments with good safety levels for clinical potential.

495 **IMRC transfusion treats lung injury and fibrosis in a dose-dependent manner**

496 To evaluate the therapeutic effects of IMRCs on lung injury and fibrosis, IMRCs were administered
497 intravenously into a bleomycin-induced model of lung injury. IMRCs ameliorated the total body weight
498 reduction in mice exposed to bleomycin (BLM)-induced lung injury, in a dose-dependent manner (Fig.
499 6B). Kaplan-Meier survival curves indicated that IMRC treatment prolonged the overall survival rates
500 (BLM group 12.5% vs. 1×10^6 IMRCs 25%, 3×10^6 IMRCs 50%, 5×10^6 IMRCs 62.5% ($P < 0.01$)) and
501 the median survival time (BLM group 11.5d vs. 1×10^6 IMRCs 15.5d, 3×10^6 IMRCs 18d, 5×10^6 IMRCs
502 21d) in mice exposed to bleomycin-induced lung injury. There was a statistically significant difference
503 between the BLM group and the 5×10^6 IMRCs group, but not the other groups (Fig. 6C). Histological
504 staining of the lung at 21 days after bleomycin injection (inflammation phase) showed diffuse pneumonic
505 lesions with loss of the normal alveolar architecture, septal thickening, enlarged alveoli, and increased
506 infiltration of inflammatory cells in the interstitial and peribronchiolar areas, in the BLM lung compared
507 with normal lung. IMRC treatment reduced alveolar thickening in the lung in a dose-dependent manner
508 (Fig. 6D-F). Moreover, IMRC treatment reduced the number of macrophage in the lung (Fig. 6F). These
509 results indicated that IMRC treatment can reduce inflammation in the lung after acute injury. Moreover,
510 IMRC treatment also improved the Ashcroft score for pulmonary fibrosis in a dose-dependent manner
511 (Fig. 6G). In particularly, IMRC treatment decreased collagen deposition in the BLM lung in a dose-

512 dependent manner (Fig. S6). The expression levels of COL I, FN and α-SMA were also significant lower
513 after IMRC treatment (Fig. S6). ELISA showed that IMRC treatment reduced both TNF-α and TGF-β1
514 levels in the BLM lung in a dose-dependent manner (Fig. 6H, I). These results suggested that IMRCs
515 can significantly reduce inflammation and fibrosis after lung injury, in a dose-dependent manner.

516 **IMRC treatment of lung injury and fibrosis is superior to UCMSCs and pirfenidone injections**

517 Pirfenidone (PFD) is an FDA-approved drug for the treatment of idiopathic pulmonary fibrosis. It works
518 by reducing lung fibrosis through downregulating the production of growth factors and procollagens I
519 and II. To evaluate the efficacy of IMRC treatment, we compared it side-by-side with UCMSCs and PFD
520 treatments of BLM-injured mice (Fig. 6J). Our results showed that IMRC treatment led to an improved
521 amelioration of the weight reduction after BLM-induced lung injury, compared to UCMSCs or PFD
522 treatments (Fig. 6K). Kaplan-Meier survival curves indicated that the IMRC treatments also resulted in
523 the highest overall survival rates compared to UCMSCs or PFD treatments (Fig. 6L; BLM group 39.02%,
524 vs. IMRCs 70% ($P<0.01$), UCMSCs 52.63%, PFD 65% ($P < 0.05$)). Moreover, IMRC treatment showed
525 the best improvement in lung morphology (Fig. S7A) and the best reduction in BLM-induced edema, as
526 measured by the lung coefficient (lung wet weight/total body weight), compared to UCMSCs or PFD
527 treatments (Fig. S7B).
528
529 Functionally, mice treated with IMRCs showed the best improvements in indices for lung capacity,
530 including pressure-volume (PV), inspiratory capacity (IC), static compliance (Crs) and forced vital
531 capacity (FVC) (Fig. S8A, B, C, D). IMRC treatment also showed the best reduction in functional indices
532 for lung fibrosis, including respiratory resistance (Rrs), elastic resistance (Ers), tissue damping (G) and
533 tissue elasticity (H) were observed (Fig. S8E, F, G, H). Computed tomography (CT) scans also showed
534 that IMRC treatment led to the best improvement in lung morphology, compared to UCMSCs or PFD
535 treatment (Fig. S8I, J). In fact, measurements of the lung volume indicated that mice treated with IMRCs
536 had the best improvement in lung volume compared to UCMSCs or PFD treatments. These results
537 indicated that the IMRC therapy is superior to primary UCMSCs and pirfenidone in treating lung injury
538 and fibrosis.
539 Encouraged by these results, we pilot-tested IMRC transfusion as compassionate treatments in two

540 severely ill COVID-19 patients who were diagnosed with ALI, as part of an expanded access program.
541 After patient consent, IMRCs were administered intravenously in both patients. Within 14 days after
542 IMRC transfusion, both the COVID-19 patients had significantly recovered from pneumonia, tested
543 negative for SARS-CoV-2, and were recommended for discharge. Cytokine analysis of both patients'
544 plasma showed very high levels of inflammatory cytokines initially in days 1-2, as expected of the ALI-
545 induced cytokine storm that occurred at the point of treatment (Fig. 6M). However, by days 4-8, many
546 pro-inflammatory cytokines were suppressed after IMRC infusion, including GRO-α, IFN-α2, IL-3, IL-
547 9, IL-13, MCP-3, M-CSF, sCD40L and TNF-α (Fig. 6M). These results confimed that IMRCs do
548 manifest a hyper-immunomodulatory function, with significant therapeutic benefits to ALI patients
549 without other treatment options.

550 **Discussion**

551 In this study, IMRCs were derived from self-renewing hESC cultures with xeno-free reagents. Our results
552 showed that IMRCs, while similar to primary UCMSCs, were superior in their proliferative capacity,
553 hyper-immunomodulatory and anti-fibrotic functions. In addition, the cell diameters of IMRCs were
554 generally smaller than UCMSCs, suggesting that they pose lower risks for pulmonary embolism after
555 injection. Detailed analysis of mice and monkeys after IMRCs injections indicates that IMRCs do not
556 engraft nor transdifferentiate nor initiate tumorigenesis, showing excellent potential for short- and long-
557 term safety profiles by a range of in vitro and in vivo assays. Most importantly, our experiments with the
558 bleomycin mouse model of lung injury showed that treatments with IMRCs are superior to primary
559 UCMSCs and the FDA-approved pirfenidone in therapeutic efficacy.
560 In recent years, MSC-like cells have been generated from hESCs using various protocols[18,19,34,35].
561 However, to the best of our knowledge and in spite of significant effort by numerous groups, previously
562 reported studies lacked biosafety-related experiments. This has hindered their translation to clinical
563 application. To ensure safety, a series of biosafety-related experiments were performed according to the
564 "Guidelines for Human Somatic Cell Therapies and Quality Control of Cell-based Products" and the
565 IMRCs were verified as suitable for use in human therapy. Our data showed that there was no teratoma
566 formation observed after IMRCs injection into the testes of NOD-SCID mice. In addition, single cell
567 RNA sequencing data showed no residual hESCs were detected in IMRCs and soft agar assays also

568 showed that no colonies were formed by IMRCs. In addition, the somatic mutation analysis by whole
569 genome sequencing also showed no mutations in proto-oncogenes and tumor suppressor genes, nor any
570 coding and non-coding exon regions of IMRCs. These results indicated that IMRCs have no
571 demonstrable potential to form tumors. Moreover, IMRCs could not undergo long-term engraftment and
572 disappeared around day 46. IMRCs did not transdifferentiate into endothelial cells nor alveolar epithelial
573 cells in the lung. To evaluate the risks of clinical application, short- and long-term toxicity tests were
574 performed in cynomolgus monkeys. After 6 months, both acute toxicity tests and long-term toxicity test
575 data showed that no abnormalities were observed. These results proved that IMRCs could have an
576 excellent safety profile and clinical potential. Moreover, the above data suggested that the therapeutic
577 efficacy of IMRCs may not be due to long-term engraftment and direct repair of tissue, but due to their
578 hyper-immunomodulatory and anti-fibrotic functions at inflammatory sites of tissue interstitium.
579 Like MSCs, the IMRCs are immunoprivileged, and can escape the immune response through their lack
580 of expression of HLA class II and their weak expression of HLA class I, thus making them valuable
581 choices for allogeneic cell therapy. Moreover, it has been reported that MSCs could release
582 immunomodulatory factors, alter the expression of surface molecules, and produce growth factors during
583 an immune response to the inflammatory cytokines produced by T cells and antigen-presenting cells[36].
584 These immunomodulatory factors are crucial for regulating the immune system and promoting tissue
585 repair. Accordingly, expression of the T cell-suppressive *IDO1* greatly increased in IMRCs after
586 stimulation with the pro-inflammatory cytokine IFN-γ, even more than UCMSCs. Genome-wide RNA
587 sequencing revealed that IMRCs and UCMSCs had different expression profiles after exposure to IFN-
588 γ. Analysis of the secretomes of IMRCs and UCMSCs confirmed at least nine pro-inflammatory
589 cytokines that were lower, and several anti-inflammatory cytokines and pro-regenerative factors that
590 were higher in IMRCs than UCMSCs. All these results suggested that IMRCs possess a hyper-
591 immunomodulatory capacity compared to primary UCMSCs, after stimulation with IFN-γ. Thus, these
592 cells can be administered to immunocompetent animals and human patients without the need for further
593 immunosuppression.
594 Moreover, higher levels of MMP1 were secreted by IMRCs than primary UCMSCs. MMP1 plays a very
595 important role in the process of fibrosis, by degrading existing collagens and promoting the early stages
596 of tissue remodeling that are critical for the progression of fibrogenesis[37,38]. In general, an imbalance
597 between MMPs and TIMPs is the direct cause of fibrosis and tissue scarring. It has been reported that

598 transplantation of human *MMP1*-overexpressing bone marrow-derived mesenchymal stem cells can
599 attenuate CCL4-induced liver fibrosis in rats[39]. Therefore, it is conceivable that IMRCs that highly
600 express MMP1 may also reverse lung fibrosis. Accordingly, our data showed that the secretome from
601 IMRCs could reduce collagen I levels during fibrogenesis induced by TGF-β1. However, it is still unclear
602 whether MMP1 played a direct role in the decrease of collagen I. Future work will focus on the role of
603 MMP1 by using *MMP1*-knockout IMRCs in vitro and in vivo.
604 The mouse BLM model is similar to human ALI/ARDS during the acute inflammatory phase. Although
605 fibroblastic foci, alveolar epithelial type 2 cells hyperplasia and honeycombing lesions are reduced
606 compared with those in humans, indicating that the reproduction of human ARDS is not complete in the
607 mouse BLM model, injury to alveolar epithelial cells has been shown to be a common contributing factor
608 to the pathogenesis of both human ARDS and BLM-induced mouse pulmonary injury[40,41]. To test the
609 therapeutic efficacy of IMRCs in the BLM mouse model, the delivery route and schedule of
610 administration (e.g. single dose versus repeated doses) was carefully considered. Intravenous infusion is
611 one of the principal delivery routes, considered to be minimally invasive, simple-to-use, and is the most
612 common mode for primary MSCs delivery in diverse lung disorders[42,43]. Furthermore, systemic
613 intravenous transplantation may be a suitable administration route in other future clinical scenarios. In
614 our present study, intravenous IMRCs improved the survival rate of mice with BLM-induced lung injury
615 in a dose-dependent manner, by inhibiting both pulmonary inflammation and fibrosis. As demonstrated
616 in vitro, IMRCs inhibited the production of pro-inflammatory cytokines and pro-fibrosis cytokines, such
617 as TNF-α and TGF-β1, in lung tissue in vivo. Furthermore, lung function indicators such as PV, IC, Rrs,
618 Crs, Ers, Rn, G, H and FVC were improved compared with the BLM group. Furthermore, pilot tests of
619 IMRC transfusion in the clinic confirmed that IMRCs could rapidly suppress the inflammatory cytokine
620 storm in two COVID-19 patients within 4-8 days, and both severely ill patients were recommended for
621 discharge within 14 days after IMRC treatment.
622 It should be noted that IMRCs were administered at 1 and 7 days after initiation of BLM-injury, but
623 before fibrosis has fully developed. In fact several studies have reported that primary MSCs treatments
624 do not improve pathologically-established pulmonary fibrosis, while some studies suggest that primary
625 MSCs actually exacerbate pulmonary fibrosis[44]. Regarding the efficacy of IMRCs in established fibrosis,
626 further studies are necessary and our own investigation is still ongoing. It is unclear whether primary
627 MSCs do promote pulmonary fibrosis, but their lack of positive therapeutic effect may be due to

differences in MSC subtypes, fibrosis stages after induction, species of model animals, and routes of administration of MSCs. Thus, clinical applications with MSCs should be considered carefully. As noted in this paper, it is important to carefully document the origin, preparation and characterization of MSC-like cells. Here we have established a substantial profile of efficacy and safety for the hESC-derived IMRCs. These efforts provide considerable grounds for hope that this artificial cell-type could provide significant clinical benefit in the treatment of fibrotic conditions.

Conclusions

In summary, our findings show that intravenously delivered IMRCs inhibited both pulmonary inflammation and fibrosis after acute lung injury in vivo. IMRCs significantly improved the survival rate in a dose-dependent manner. Furthermore, the mechanism for amelioration of pulmonary injury may be mediated by the IMRCs' paracrine action rather than their potential to differentiate and replace the damaged alveolar epithelial cells. The IMRCs' functional inhibition of TGF-β1-induced fibrosis could also be part of its mechanism. IMRCs were superior to UCMSCs and pirfenidone in therapeutic efficacy against lung injury and fibrosis. Furthermore, IMRCs showed an excellent safety profile in both mice and monkeys. In light of recent public health crises involving pneumonia, respiratory failure, ALI and ARDS, our pre-clinical results indicate that IMRCs are ready to be carefully considered for human trials in the treatment of lung injury and fibrosis.

Acknowledgements

This work was supported by Beijing Municipal Science & Technology Commission (Z181100003818005 to Q.Z.), National Key Research and Development Program (2018YFA0108400 and 2017YFA0104403 to J.H., 2017YFA0105001, 2016YFA0101502 to L.W.), the Strategic Priority Research Program of the Chinese Academy of Sciences (XDA16030601 to L.W., XDA16040502 to J.H.), the National Natural Science Foundation of China (31621004 to Q.Z. and W.L.), the Key Research Projects of the Frontier Science of the Chinese Academy of Sciences (QYZDY-SSW-SMC002 to Q.Z.), and China Postdoctoral Science Foundation (2019M660791 to L.W.).

Author contributions

Liu Wang, Baoyang Hu, Huaping Dai and Jie Hao conceived the project and supervised the experiments. Jun Wu, Dingyun Song and Zhongwen Li completed majority of the experiments. Jun Wu, Dingyun Song and Zhongwen Li wrote the manuscript with help from all the authors. Jun Wu, Dingyun Song, Zhongwen Li, Baojie Guo, Yani Xiao, Wenjing Liu, Lingmin Liang, Chunjing Feng, Tingting Gao, Zai Wang, Jianyan Wen, Shengnan Yang, Peipei Liu, Lei Wang, Yukai Wang, Liang Peng, Guihai Feng, Shiqiang Huang, Glyn Nigel Stacey, Wei Li, Yan Huo, Ronghua Jin, Qi Zhou, Liu Wang, Baoyang Hu, Huaping Dai and Jie Hao participated in the experiments and data analysis.

Conflict of interest

The authors declare no conflict of interest.

References

1 Yang, J. & Jia, Z. Cell-based therapy in lung regenerative medicine. *Regenerative medicine research* **2**, 7, doi:10.1186/2050-490x-2-7 (2014).

2 Fan, E., Brodie, D. & Slutsky, A. S. Acute Respiratory Distress Syndrome: Advances in Diagnosis and Treatment. *Jama* **319**, 698-710, doi:10.1001/jama.2017.21907 (2018).

3 Rubenfeld, G. D. *et al.* Incidence and outcomes of acute lung injury. *N Engl J Med* **353**, 1685-1693, doi:10.1056/NEJMoa050333 (2005).

4 Bellani, G. *et al.* Epidemiology, Patterns of Care, and Mortality for Patients With Acute Respiratory Distress Syndrome in Intensive Care Units in 50 Countries. *Jama* **315**, 788-800, doi:10.1001/jama.2016.0291 (2016).

5 Hamacher, J. *et al.* Tumor necrosis factor-alpha and angiostatin are mediators of endothelial cytotoxicity in bronchoalveolar lavages of patients with acute respiratory distress syndrome. *Am J Respir Crit Care Med* **166**, 651-656, doi:10.1164/rccm.2109004 (2002).

6 Raghu, G. *et al.* An official ATS/ERS/JRS/ALAT statement: idiopathic pulmonary fibrosis: evidence-based guidelines for diagnosis and management. *Am J Respir Crit Care Med* **183**, 788-824, doi:10.1164/rccm.2009-040GL (2011).

7 Marshall, R., Bellingan, G. & Laurent, G. The acute respiratory distress syndrome: fibrosis in the fast lane. *Thorax* **53**, 815-817, doi:10.1136/thx.53.10.815 (1998).

8 Dhainaut, J. F., Charpentier, J. & Chiche, J. D. Transforming growth factor-beta: a mediator of cell regulation in acute respiratory distress syndrome. *Critical care medicine* **31**, S258-264, doi:10.1097/01.Ccm.0000057901.92381.75 (2003).

9 King, T. E., Jr. *et al.* A phase 3 trial of pirfenidone in patients with idiopathic pulmonary fibrosis. *N Engl J Med* **370**, 2083-2092, doi:10.1056/NEJMoa1402582 (2014).

10 Yoon, H. Y., Park, S., Kim, D. S. & Song, J. W. Efficacy and safety of nintedanib in advanced idiopathic pulmonary fibrosis. *Respiratory research* **19**, 203, doi:10.1186/s12931-018-0907-8 (2018).

11 Zhou, H., Liu, M. & Lyu, X. [Research progress of mesenchymal stem cells in the treatment of

ALI]. *Zhonghua wei zhong bing ji jiu yi xue* **29**, 1039-1042, doi:10.3760/cma.j.issn.2095-4352.2017.11.017 (2017).

12 Serrano-Mollar, A. Cell Therapy in Idiopathic Pulmonary Fibrosis(†). *Med Sci (Basel)* **6**, 64, doi:10.3390/medsci6030064 (2018).

13 Ortiz, L. A. *et al.* Interleukin 1 receptor antagonist mediates the antiinflammatory and antifibrotic effect of mesenchymal stem cells during lung injury. *Proceedings of the National Academy of Sciences of the United States of America* **104**, 11002-11007, doi:10.1073/pnas.0704421104 (2007).

14 Walter, J., Ware, L. B. & Matthay, M. A. Mesenchymal stem cells: mechanisms of potential therapeutic benefit in ARDS and sepsis. *Lancet Respir Med* **2**, 1016-1026, doi:10.1016/s2213-2600(14)70217-6 (2014).

15 G, W. J. *et al.* Mesenchymal stem (stromal) cells for treatment of ARDS: a phase 1 clinical trial. *The Lancet. Respiratory medicine* **3** (2015).

16 Thomson, J. A. *et al.* Embryonic stem cell lines derived from human blastocysts. *Science (New York, N.Y.)* **282**, 1145-1147, doi:10.1126/science.282.5391.1145 (1998).

17 Barberi, T., Willis, L. M., Socci, N. D. & Studer, L. Derivation of multipotent mesenchymal precursors from human embryonic stem cells. *PLoS medicine* **2**, e161, doi:10.1371/journal.pmed.0020161 (2005).

18 Hwang, N. S. *et al.* In vivo commitment and functional tissue regeneration using human embryonic stem cell-derived mesenchymal cells. *Proceedings of the National Academy of Sciences of the United States of America* **105**, 20641-20646, doi:10.1073/pnas.0809680106 (2008).

19 Vodyanik, M. A. *et al.* A mesoderm-derived precursor for mesenchymal stem and endothelial cells. *Cell stem cell* **7**, 718-729, doi:10.1016/j.stem.2010.11.011 (2010).

20 Gu, Q. *et al.* Accreditation of Biosafe Clinical-Grade Human Embryonic Stem Cells According to Chinese Regulations. *Stem cell reports* **9**, 366-380, doi:10.1016/j.stemcr.2017.04.017 (2017).

21 Pittenger, M. F. *et al.* Multilineage potential of adult human mesenchymal stem cells. *Science (New York, N.Y.)* **284**, 143-147, doi:10.1126/science.284.5411.143 (1999).

22 Han, X. *et al.* Mapping human pluripotent stem cell differentiation pathways using high throughput single-cell RNA-sequencing. *Genome biology* **19**, 47, doi:10.1186/s13059-018-1426-0 (2018).

23 Kim, D., Langmead, B. & Salzberg, S. L. HISAT: a fast spliced aligner with low memory requirements. *Nature methods* **12**, 357-360, doi:10.1038/nmeth.3317 (2015).

24 Trapnell, C. *et al.* Transcript assembly and quantification by RNA-Seq reveals unannotated transcripts and isoform switching during cell differentiation. *Nature biotechnology* **28**, 511-515, doi:10.1038/nbt.1621 (2010).

25 Subramanian, A. *et al.* Gene set enrichment analysis: a knowledge-based approach for interpreting genome-wide expression profiles. *Proceedings of the National Academy of Sciences of the United States of America* **102**, 15545-15550, doi:10.1073/pnas.0506580102 (2005).

26 Prasad, V. K. *et al.* Efficacy and safety of ex vivo cultured adult human mesenchymal stem cells (Prochymal) in pediatric patients with severe refractory acute graft-versus-host disease in a compassionate use study. *Biology of blood and marrow transplantation : journal of the American Society for Blood and Marrow Transplantation* **17**, 534-541,

734 doi:10.1016/j.bbmt.2010.04.014 (2011).
735 27 Horibata, S., Vo, T. V., Subramanian, V., Thompson, P. R. & Coonrod, S. A. Utilization of the
736 Soft Agar Colony Formation Assay to Identify Inhibitors of Tumorigenicity in Breast Cancer
737 Cells. *Journal of visualized experiments : JoVE*, e52727, doi:10.3791/52727 (2015).
738 28 Zhang, W. *et al.* SIRT6 deficiency results in developmental retardation in cynomolgus monkeys.
739 *Nature* **560**, 661-665, doi:10.1038/s41586-018-0437-z (2018).
740 29 Quinlan, A. R. & Hall, I. M. BEDTools: a flexible suite of utilities for comparing genomic
741 features. *Bioinformatics (Oxford, England)* **26**, 841-842, doi:10.1093/bioinformatics/btq033
742 (2010).
743 30 Yang, J. *et al.* Tumor tropism of intravenously injected human-induced pluripotent stem cell-
744 derived neural stem cells and their gene therapy application in a metastatic breast cancer model.
745 **30**, 1021-1029 (2012).
746 31 P, M. *et al.* Fluorescence molecular tomography of DiR-labeled mesenchymal stem cell
747 implants for osteochondral defect repair in rabbit knees.%A Berninger MT. **27**, 1105-1113
748 (2017).
749 32 L, L., HT, M., JH, B. & physiology, I. C. J. J. o. a. Nonlinearity of respiratory mechanics during
750 bronchoconstriction in mice with airway inflammation.%A Wagers S. **92**, 1802-1807 (2002).
751 33 Overmyer, K. A., Thonusin, C., Qi, N. R., Burant, C. F. & Evans, C. R. J. P. O. Impact of
752 Anesthesia and Euthanasia on Metabolomics of Mammalian Tissues: Studies in a C57BL/6J
753 Mouse Model. **10**, e0117232 (2015).
754 34 Lian, Q. *et al.* Derivation of clinically compliant MSCs from CD105+, CD24- differentiated
755 human ESCs. *Stem cells (Dayton, Ohio)* **25**, 425-436, doi:10.1634/stemcells.2006-0420 (2007).
756 35 Lee, E. J. *et al.* Novel embryoid body-based method to derive mesenchymal stem cells from
757 human embryonic stem cells. *Tissue engineering. Part A* **16**, 705-715,
758 doi:10.1089/ten.tea.2008.0596 (2010).
759 36 Shi, Y. *et al.* How mesenchymal stem cells interact with tissue immune responses. *Trends in*
760 *immunology* **33**, 136-143, doi:10.1016/j.it.2011.11.004 (2012).
761 37 Milani, S. *et al.* Differential expression of matrix-metalloproteinase-1 and -2 genes in normal
762 and fibrotic human liver. *The American journal of pathology* **144**, 528-537 (1994).
763 38 Benyon, R. C., Iredale, J. P., Goddard, S., Winwood, P. J. & Arthur, M. J. Expression of tissue
764 inhibitor of metalloproteinases 1 and 2 is increased in fibrotic human liver. *Gastroenterology*
765 **110**, 821-831, doi:10.1053/gast.1996.v110.pm8608892 (1996).
766 39 Du, C. *et al.* Transplantation of human matrix metalloproteinase-1 gene-modified bone marrow-
767 derived mesenchymal stem cell attenuates CCL4-induced liver fibrosis in rats. *International*
768 *journal of molecular medicine* **41**, 3175-3184, doi:10.3892/ijmm.2018.3516 (2018).
769 40 B, I., M, C., M, O., F, V. & research, R. L. J. R. Idiopathic pulmonary fibrosis: pathogenesis and
770 management.%A Sgalla G. **19**, 32 (2018).
771 41 Betensley, A., Sharif, R. & Karamichos, D. J. J. o. C. M. A Systematic Review of the Role of
772 Dysfunctional Wound Healing in the Pathogenesis and Treatment of Idiopathic Pulmonary
773 Fibrosis. **6**, 2 (2017).
774 42 Q, H., A, M., XM, F. & Respirology, L. J. J. Adult stem cells for acute lung injury: remaining
775 questions and concerns.%A Zhu YG. **18**, 744-756 (2013).
776 43 Kanelidis, A. J., Premer, C., Lopez, J., Balkan, W. & Hare, J. M. J. C. R. Route of Delivery
777 Modulates the Efficacy of Mesenchymal Stem Cell Therapy for Myocardial Infarction: A Meta-

Analysis of Preclinical Studies and Clinical Trials. **120**, 1139 (2017).

44 Weiss, D. J., Ortiz, L. A., %J American Journal of Respiratory & Medicine, C. C. Cell therapy trials for lung diseases: progress and cautions. **188**, 123-125 (2013).

782 **Figure legends**

Figure 1

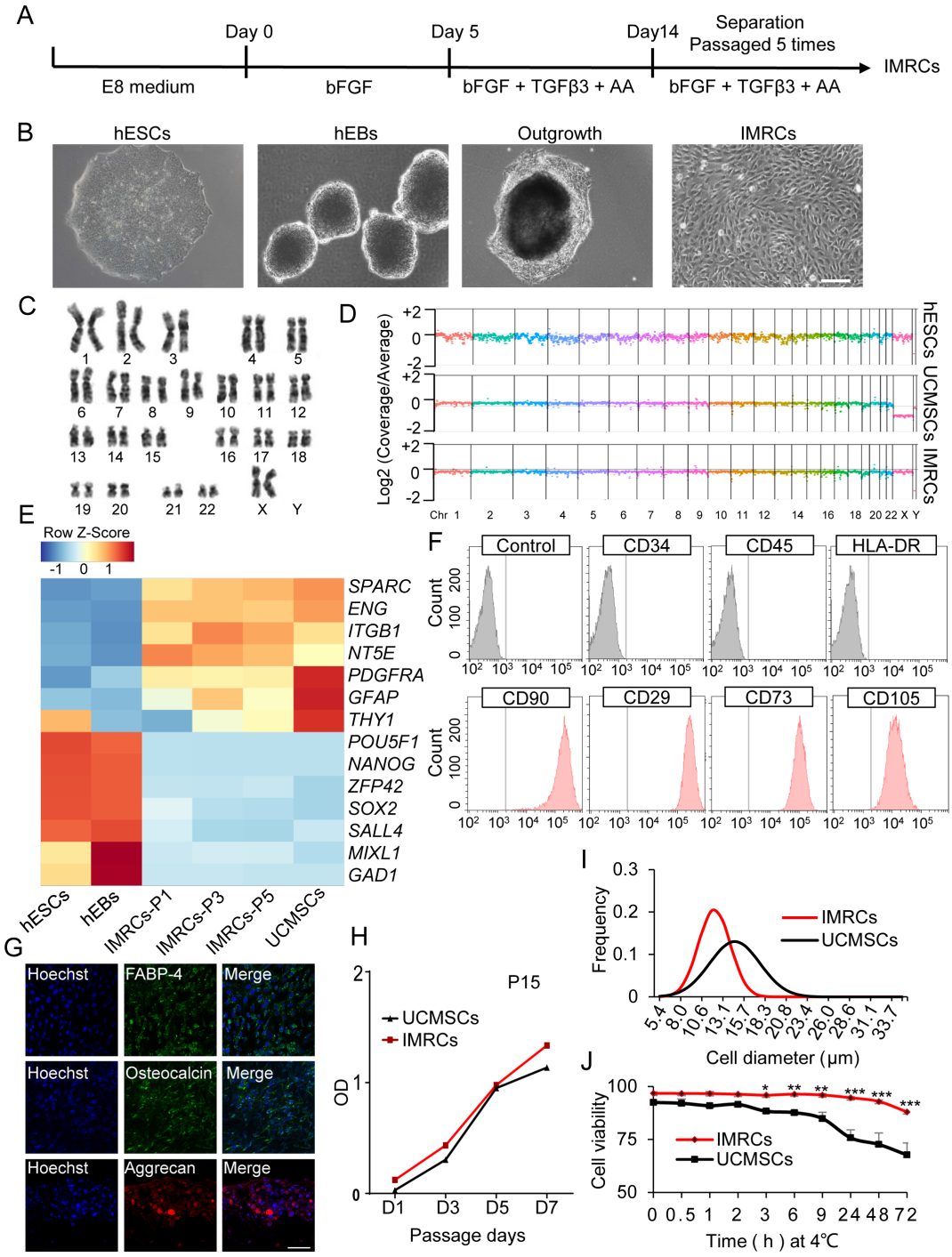

783

784 **Fig. 1 Derivation of immunity- and matrix-regulatory cells (IMRCs) from human embryonic stem**

785 **cells (hESCs).**

786 **A** Different phase of the IMRCs derivation protocol. AA, L-ascorbic acid. **B** Representative morphology

787 of cells at different stages observed by phase contrast microscopy. hEBs, human embryoid bodies. Scale

788 bars, 100 μm. **C** A representative chromosome spread of normal diploid IMRCs with 22 pairs of

789 autosomes and two X chromosomes. **D** Copy number variation (CNV) analysis by whole genome
790 sequencing for hESCs, primary UCMSCs and IMRCs. UCMSCs, umbilical cord mesenchymal stem
791 cells. **E** Heatmap showing MSC-specific marker and pluripotency marker gene expression changes, from
792 hESCs and hEBs to IMRCs at passages 1-5 (P1-5), and primary UCMSCs. **F** IMRCs' expression of
793 MSC-specific surface markers was determined by flow cytometry. Isotype control antibodies were used
794 as controls for gating. Like MSCs, the IMRCs are $CD34^-$ $CD45^-$ $HLA\text{-}DR^-$ $CD90^+$ $CD29^+$ $CD73^+$ $CD105^+$
795 cells. **G** Representative immunofluorescence staining of IMRCs after they were induced to undergo
796 adipogenic differentiation (FABP-4), osteogenic differentiation (Osteocalcin), and chondrogenic
797 differentiation (Aggrecan). Scale bars, 100 μm. **H** Proliferation curve of IMRCs and UCMSCs at the
798 15th passage. **I** Distribution of cell diameters of IMRCs and UCMSCs. **J** Viability of IMRCs and
799 UCMSCs in clinical injection buffer over time at 4°C. * $p < 0.05$, ** $p < 0.01$, *** $p < 0.001$; data are
800 represented as the mean ± SEM.

Figure 2

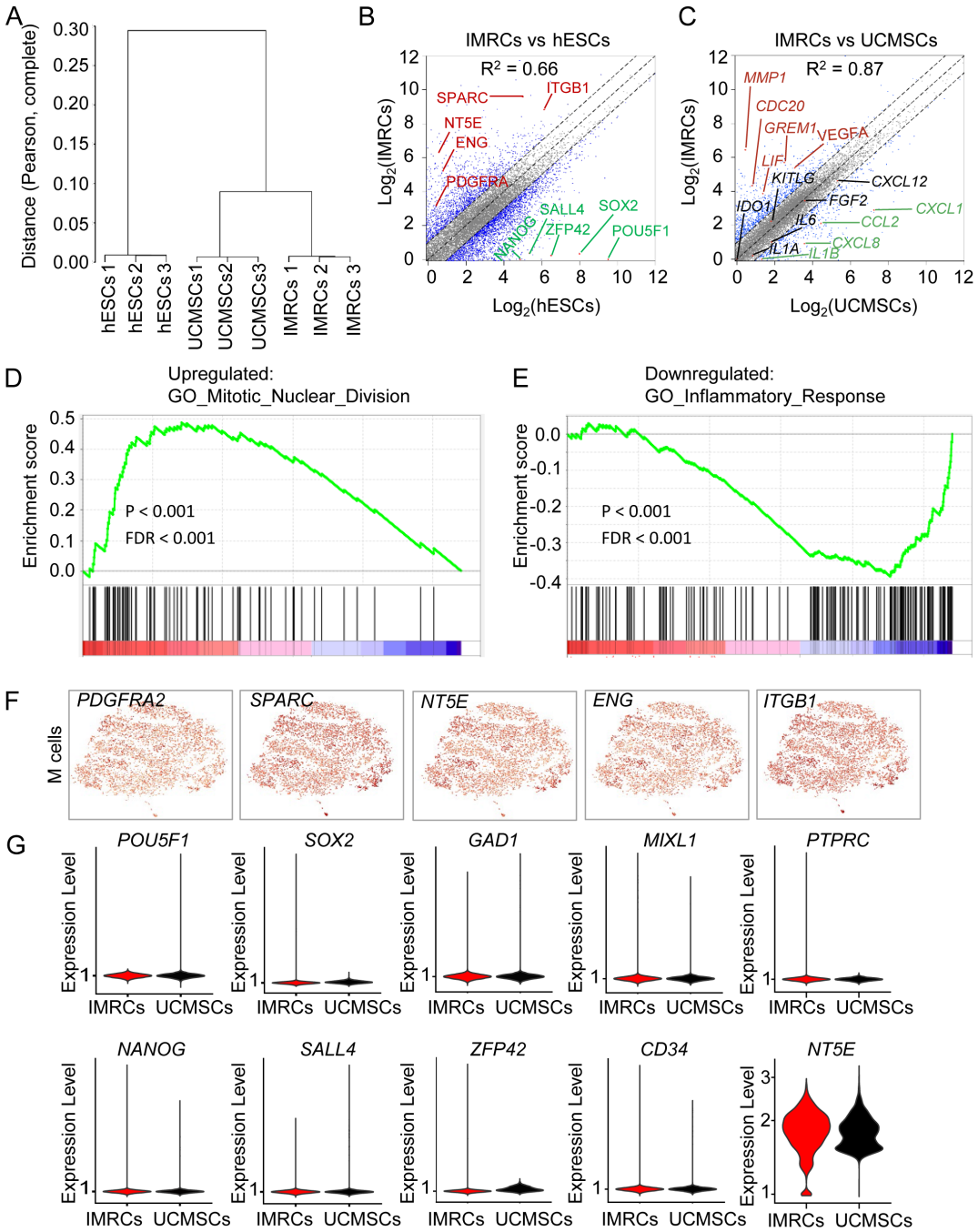

Fig. 2 IMRCs possess unique gene expression characteristics.

A Unsupervised hierarchical clustering analysis based on the Pearson correlation distance between the whole mRNA profile of each cell type. **B** Scatter plot displaying the differentially expressed genes (DEGs) between IMRCs and hESCs. Up-regulated genes are highlighted in red. Down-regulated genes are highlighted in green. Gray dots represent non-DEGs (< 2-fold change). **C** Scatter plot displaying the DEGs between IMRCs and primary UCMSCs. Up-regulated genes are highlighted in red. Down-

808 regulated genes are highlighted in green. Gray dots represent non-DEGs (< 2-fold change). **D** Gene set
809 enrichment analysis (GSEA) of the top up-regulated gene signature in IMRCs, compared with primary
810 UCMSCs. **E** GSEA of the top down-regulated gene signature in IMRCs, compared with UCMSCs. **F**
811 Heatmaps of specific gene expression amongst single IMRCs groups. **G** Quantification of non-
812 mesenchymal marker gene expression amongst single IMRCs, UCMSCs and hESCs, as measured by
813 single cell RNAseq.

Figure 3

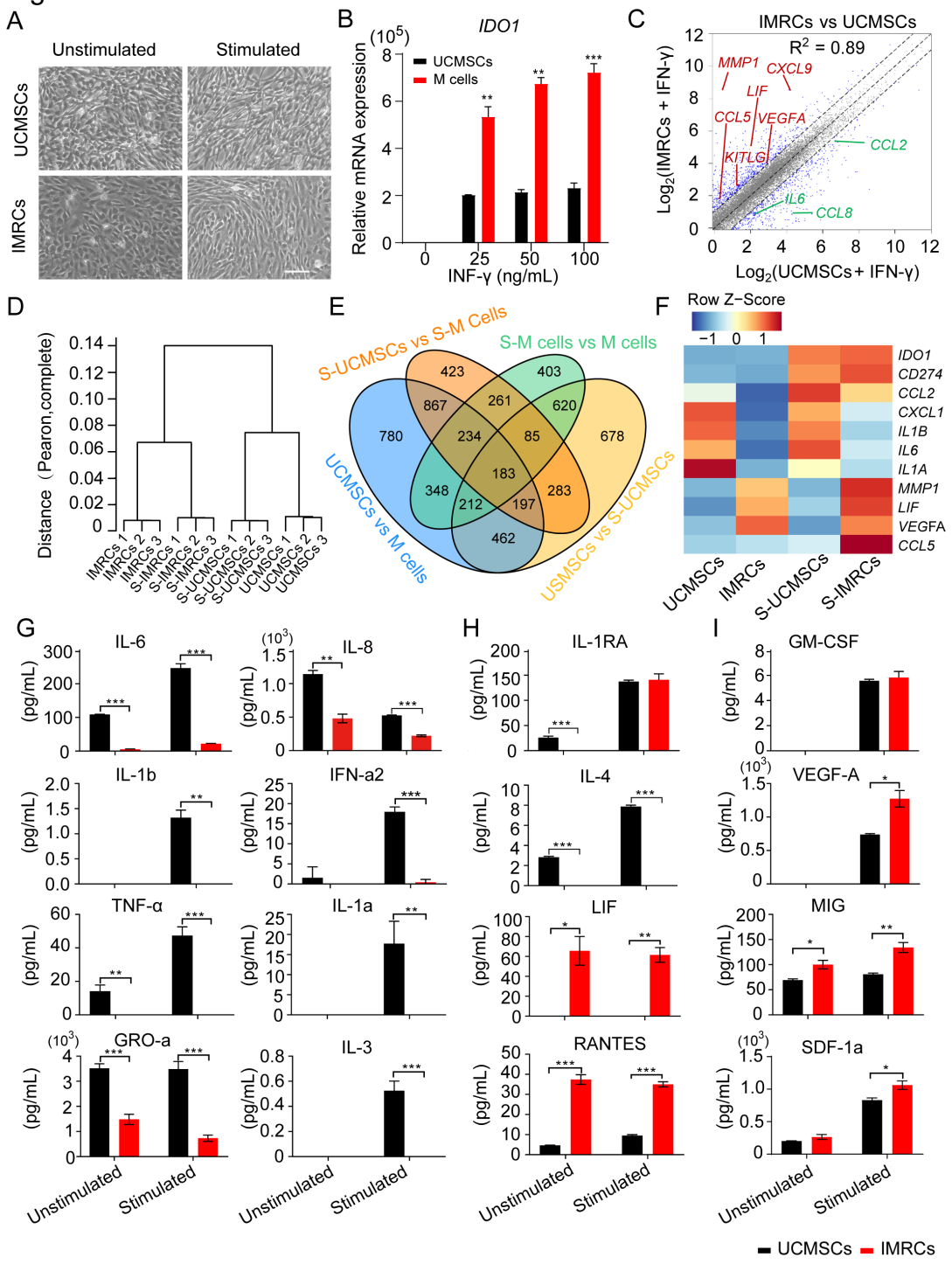

814

Fig. 3 IMRCs activated by IFN-γ show hyper-immunomodulatory potency.

A Morphology of UCMSCs and IMRCs before and after IFN-γ (100 ng/mL) stimulation. **B** Quantitative PCR for *IDO1* mRNA in UCMSCs and IMRCs before and after IFN-γ (0, 25, 50, 100 ng/mL) treatment. *GAPDH* was used for internal normalization. **C** Scatter plot displaying the DEGs between UCMSCs and IMRCs after treatment with 100 ng/mL IFN-γ. Up-regulated genes are highlighted in red. Down-regulated genes are highlighted in green. Gray dots represent non-DEGs (< 2-fold change). **D** Unsupervised hierarchical clustering analysis of UCMSCs and IMRCs, before and after IFN-γ stimulation (S-UCMSCs and S-IMRCs). **E** Venn diagram shows the overlap among UCMSC- and IMRCs -associated genes, before and after IFN-γ stimulation (S). **F** Heatmap illustrating the expression of cytokines in UCMSCs and IMRCs, before and after IFN-γ stimulation (S). **G-I** ELISA analysis of biologically relevant chemokines and cytokines in the secretome of unstimulated or stimulated IMRCs and UCMSCs. Pro-inflammatory (G), immunomodulatory (H), and pro-regenerative (I) cytokines. * $p < 0.05$, ** $p < 0.01$, *** $p < 0.001$; data are represented as the mean ± SEM. Scale bar, 100 μm.

Figure 4

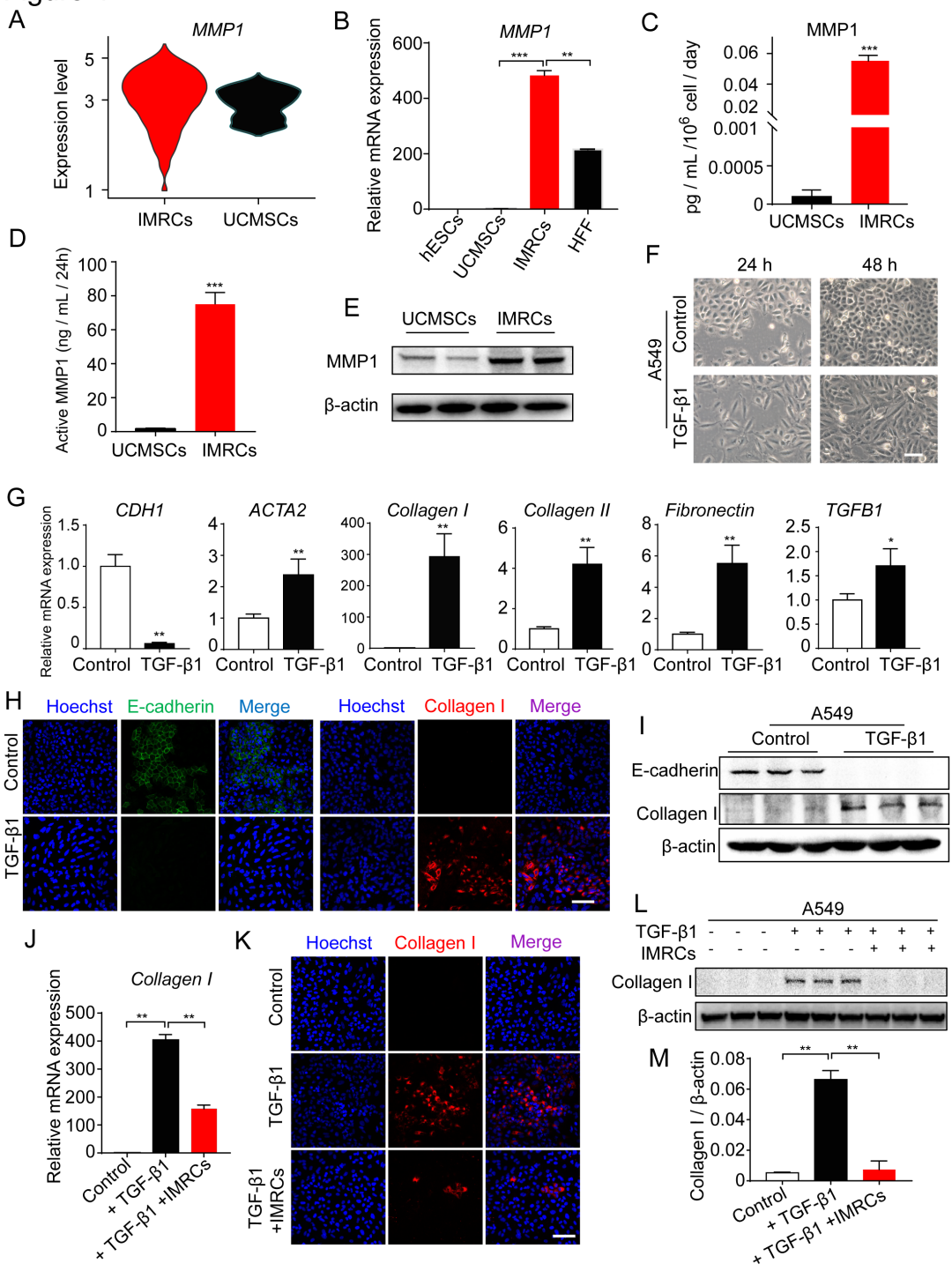

Fig. 4 IMRCs reduce the pro-fibrotic effects of TGF-β1.

A Quantification of *MMP1* gene expression amongst single IMRCs, UCMSCs and hESCs, as measured by single cell RNAseq. **B** Quantitative PCR for *MMP1* mRNA in hESCs, UCMSCs, IMRCs and human foreskin fibroblasts (HFF). **C** ELISA for MMP1 protein in the conditioned media of IMRCs and UCMSCs. **D** MMP1 activity in the conditioned media of IMRCs and UCMSCs. **E** Western blot for MMP1 protein in IMRCs and UCMSCs. β-actin was used as a loading control. **F** Representative

835 morphology of A549 cells, with or without 10 ng/mL TGF-β1 treatment for 48 h. **G** Quantitative PCR
836 for the relative expression of *CDH1*, *ACTA2*, *Collagen I*, *Collagen II, Fibronectin* and *TGFB1* mRNA in
837 A549 cells, with or without TGF-β1 treatment for 48 h. **H** Immunofluorescence staining for E-cadherin
838 and Collagen I expression in A549 cells, with or without 10 ng/mL TGF-β1 treatment for 48 h. **I** Western
839 blot for E-cadherin and Collagen I protein expression in A549 cells, with or without 10 ng/mL TGF-β1
840 treatment for 48h. **J** Quantitative PCR for *Collagen I* mRNA in A549 cells, with or without 10 ng/mL
841 TGF-β1 and IMRCs conditioned media treatment for 48 h. **K** Immunofluorescence staining for E-
842 cadherin and Collagen I expression in A549 cells, with or without 10 ng/mL TGF-β1 and IMRCs
843 conditioned media treatment for 48 h. **L** Western blot for E-cadherin and Collagen I protein expression
844 in A549 cells, with or without 10 ng/mL TGF-β1 and IMRCs conditioned media treatment for 48 h. **M**
845 Quantification of the relative Collagen I protein expression levels in **L**. * $p < 0.05$, ** $p < 0.01$, *** $p <$
846 0.001; data are represented as the mean ± SEM. Scale bar, 100 μm.

Figure 5

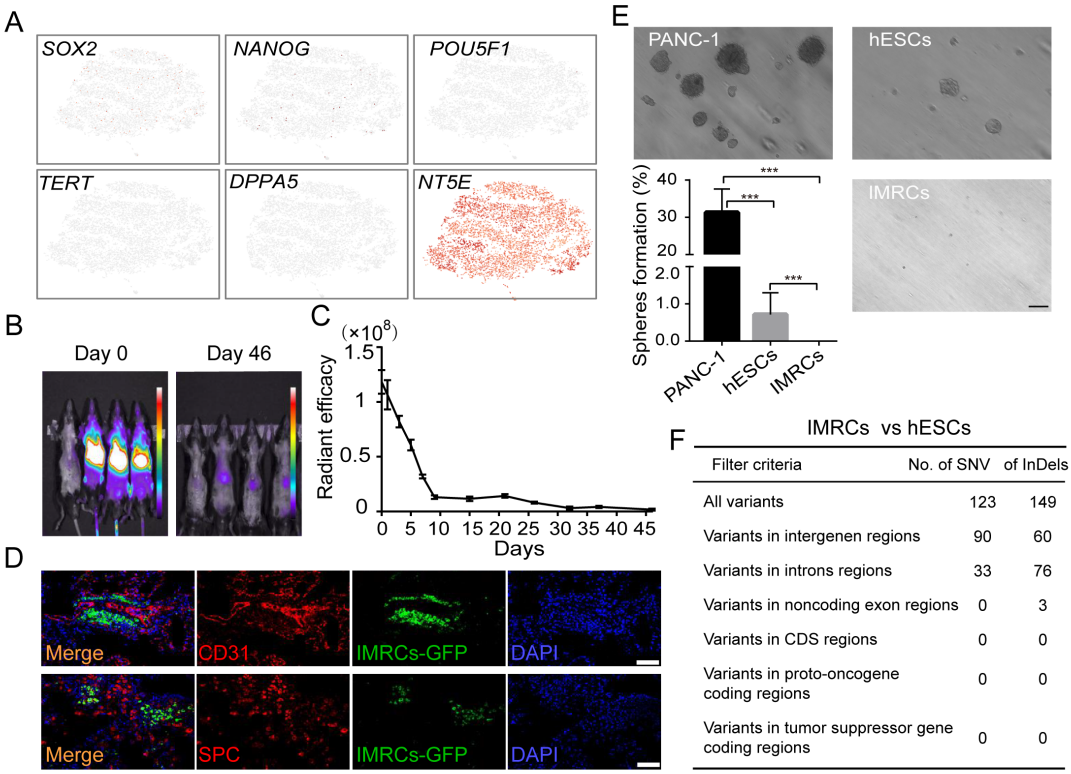

F

IMRCs vs hESCs

Filter criteria	No. of SNV	of InDels
All variants	123	149
Variants in intergenen regions	90	60
Variants in introns regions	33	76
Variants in noncoding exon regions	0	3
Variants in CDS regions	0	0
Variants in proto-oncogene coding regions	0	0
Variants in tumor suppressor gene coding regions	0	0

G Acute toxicity test in cynomolgus monkeys: blood biochemistry (after six months)

Group	ALT (U/L)	AST (U/L)	ALP (U/L)	CK (U/L)	GGT (U/L)	LDH (U/L)	TBIL (μmol/L)	BUN (mmol/L)	CRE (μmol/L)	GLU (mmol/L)	CHO (mmol/L)	TG (mmol/L)
1×10^8	55.00	30.00	165.00	123.00	65.00	497.00	3.00	6.00	58.00	5.00	3.00	1.00
0.26×10^8	73.00	34.00	160.00	164.00	38.54	330.00	3.17	8.00	61.00	4.05	3.83	0.32
0.026×10^8	63.00	49.00	94.00	317.00	51.64	298.00	5.89	7.60	71.00	2.57	2.60	0.32

Group	TP (g/L)	ALB (g/L)	A/G	IgA (g/L)	IgG (g/L)	IgM (g/L)	C3 (g/L)	C4 (g/L)	K^+ (mmol/L)	Na^+ (mmol/L)	Cl^- (mmol/L)
1×10^8	71.00	42.00	1.00	1.00	6.00	1.00	1.00	0.00	3.00	146.00	108.00
0.26×10^8	72.20	42.60	1.44	1.79	7.48	0.76	0.93	0.14	3.62	145.4	98.00
0.026×10^8	78.70	40.90	1.08	2.81	10.81	0.73	0.96	0.09	3.45	146.8	99.80

H Acute toxicity test in cynomolgus monkeys: urinalysis (after six months)

Group	GLU (mmol/L)	PRO (mg/L)	BIL (μmol/L)	URO (μmol/L)	PH	SG	ERY (mg/L)	KET (mmol/L)	NIT	Color
1×10^8	-	-	-	Normal	8.5	<1.005	-	-	-	Light yellow
0.26×10^8	-	+-	-	Normal	8.5	1.015	-	-	-	Yellow
0.026×10^8	-	-	-	Normal	8.0	1.015	-	-	1+	Colorless

Fig. 5 Evaluation of the safety of IMRC transfusion.

A t-SNE projection of single cells and their pluripotency gene expression amongst IMRCs. **B** In vivo imaging of the far red fluorescence in mice after injection of DiR-labeled IMRCs. **C** Quantification of the DiR fluorescent radiance in the whole body over time. **D** Immunofluorescence staining of lung sections for the endothelial marker CD31 and the alveolar epithelial marker SPC, 21 days after injecting GFP-labeled IMRCs. Scale bar, 100 μm. **E** Soft agar colony formation assay for the tumorigenic potential

854 of IMRCs, relative to PANC-1 cancer cells and hESCs. Scale bar, 100 μm. **F** Single nucleotide variants
855 (SNVs) and insertions/deletions (InDels) in the non-repeat regions of the IMRCs genome, relative to
856 hESCs. **G** Blood biochemistry results of cynomolgus monkeys (*Macaca fascicularis*) injected with a low
857 (2.6×10^6), medium (2.6×10^7) or high (1×10^8) dose of IMRCs after six months. AST, aspartate
858 aminotransferase; ALT, alanine aminotransferase; ALP, alkaline phosphatase; CK, creatine
859 phosphokinase; GGT, glutamyltransferase; LDH, lactate dehydrogenase; TBIL, total bilirubin; BUN,
860 urea nitrogen; CRE, creatinine; GLU, glucose; CHO, total cholesterol; TG, triglyceride; TP, total protein;
861 ALB, albumin ; A/G, albumin/globulin. **H** Urinalysis results of cynomolgus monkeys (*Macaca*
862 *fascicularis*) injected with a low (2.6×10^6), medium (2.6×10^7) or high (1×10^8) dose of IMRCs after six
863 months. PRO, urine protein; BIL, urine bilirubin; URO, urinary gallbladder; SG, specific gravity; ERY,
864 erythrocyte; KET, ketone; NIT, nitrite. * $p < 0.05$, ** $p < 0.01$, *** $p < 0.001$; data are represented as the
865 mean ± SEM.

Figure 6

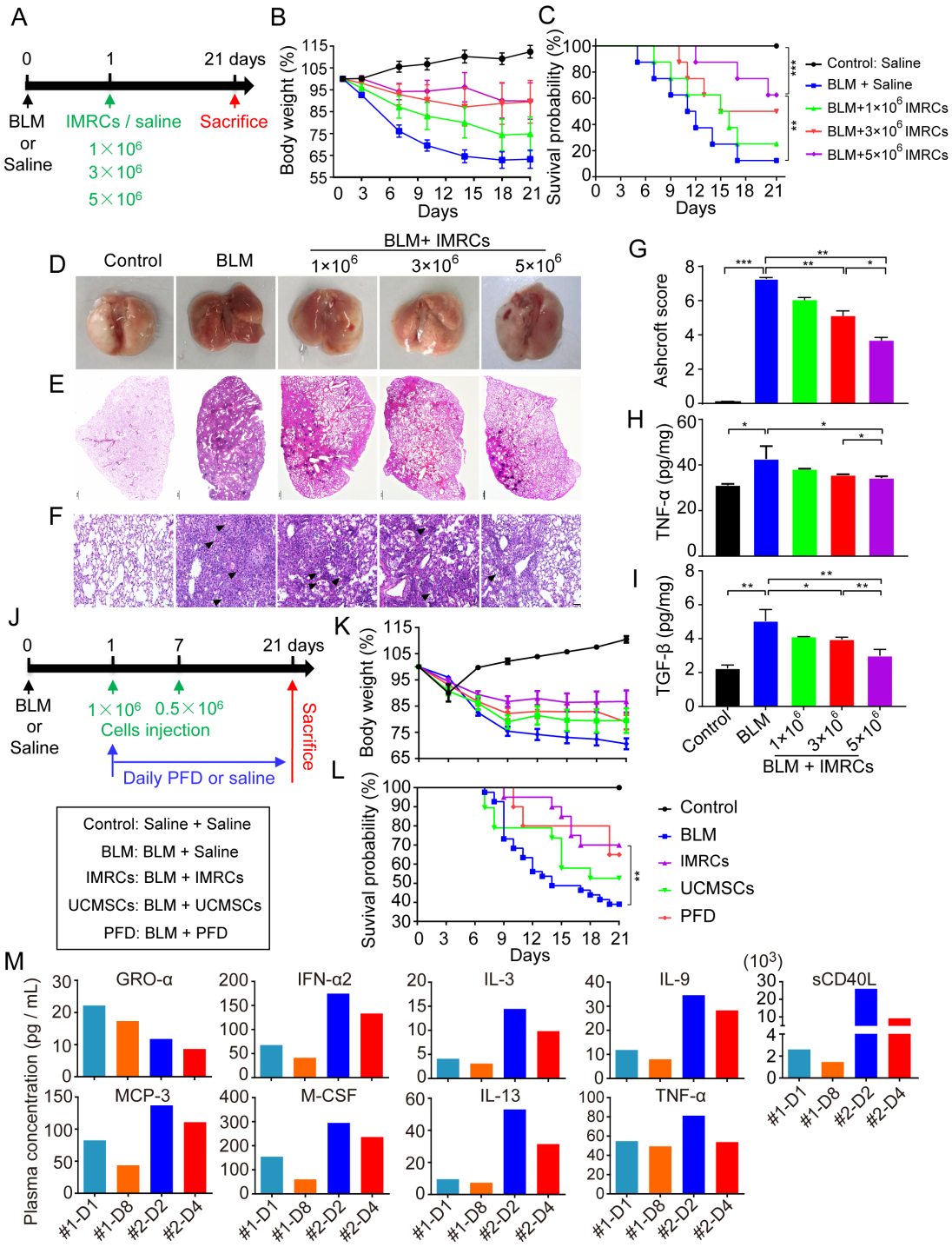

Fig. 6 IMRC transfusion treats lung injury and fibrosis dose-dependently.

A Diagram of the animal experimental protocol for dose escalation. Mice received intratracheal bleomycin (BLM; 2.5 mg/kg body weight) or the same amount of saline at day 0. At day 1, some BLM-injured mice received an intravenous (I.V.) injection of 1×10^6, 3×10^6 or 5×10^6 IMRCs via the caudal vein. A group of BLM-injured mice and normal control mice received the same volume of saline. Mice were randomly grouped (n=8 per group). **B** Relative body weight (%) changes of the mice receiving

different interventions. **C** Kaplan-Meier survival curves of the mice receiving different interventions. **D** Representative images of whole lungs from all groups at 21 days post-injury. **E, F** Representative histology of lung sections stained with H&E (Scale bar, 500 μm and 50 μm) at 21 days post-injury. Arrowheads, inflammatory infiltration. **G** Quantitative evaluation of fibrotic changes with the Ashcroft score in lungs of mice receiving different interventions. The Ashcroft scores based on the lung H&E sections. The severity of fibrotic changes in each section was assessed as the mean score of severity in the observed microscopic fields. Six fields per section were analyzed. **H-I** ELISA for the protein levels of TNF-α and TGF-β1 in the lungs of mice receiving different interventions. **J** Diagram of the animal experimental protocol for multiple arm testing. Double I.V. injections of 1×10^6 and 0.5×10^6 IMRCs (at days 1 and 7 respectively) were compared side-by-side with double I.V. injections of 1×10^6 and 0.5×10^6 UCMSCs (at days 1 and 7 respectively), vs. daily pirfenidone (PFD) or saline treatments of mice injured with intratracheal bleomycin (BLM; 2.5 mg/kg body weight) at day 0. **K** Relative body weight (%) changes of mice receiving different interventions. **L** Kaplan-Meier survival curves of mice receiving different interventions. **M** ELISA analysis of pro-inflammatory cytokines in the plasma of two ALI patients after intravenous IMRC transfusion. * $p < 0.05$, ** $p < 0.01$, *** $p < 0.001$; data are represented as the mean ± SEM.